Title
Asymmetric mechanism of molecular chaperone Hsp90

Author
Elnatan, Daniel

Publication Date
2017

Peer reviewed|Thesis/dissertation

Asymmetric mechanism of molecular chaperone Hsp90

by

Daniel Elnatan

DISSERTATION

Submitted in partial satisfaction of the requirements for the degree of

DOCTOR OF PHILOSOPHY

in

Biochemistry and Molecular Biology

in the

GRADUATE DIVISION

of the

UNIVERSITY OF CALIFORNIA, SAN FRANCISCO

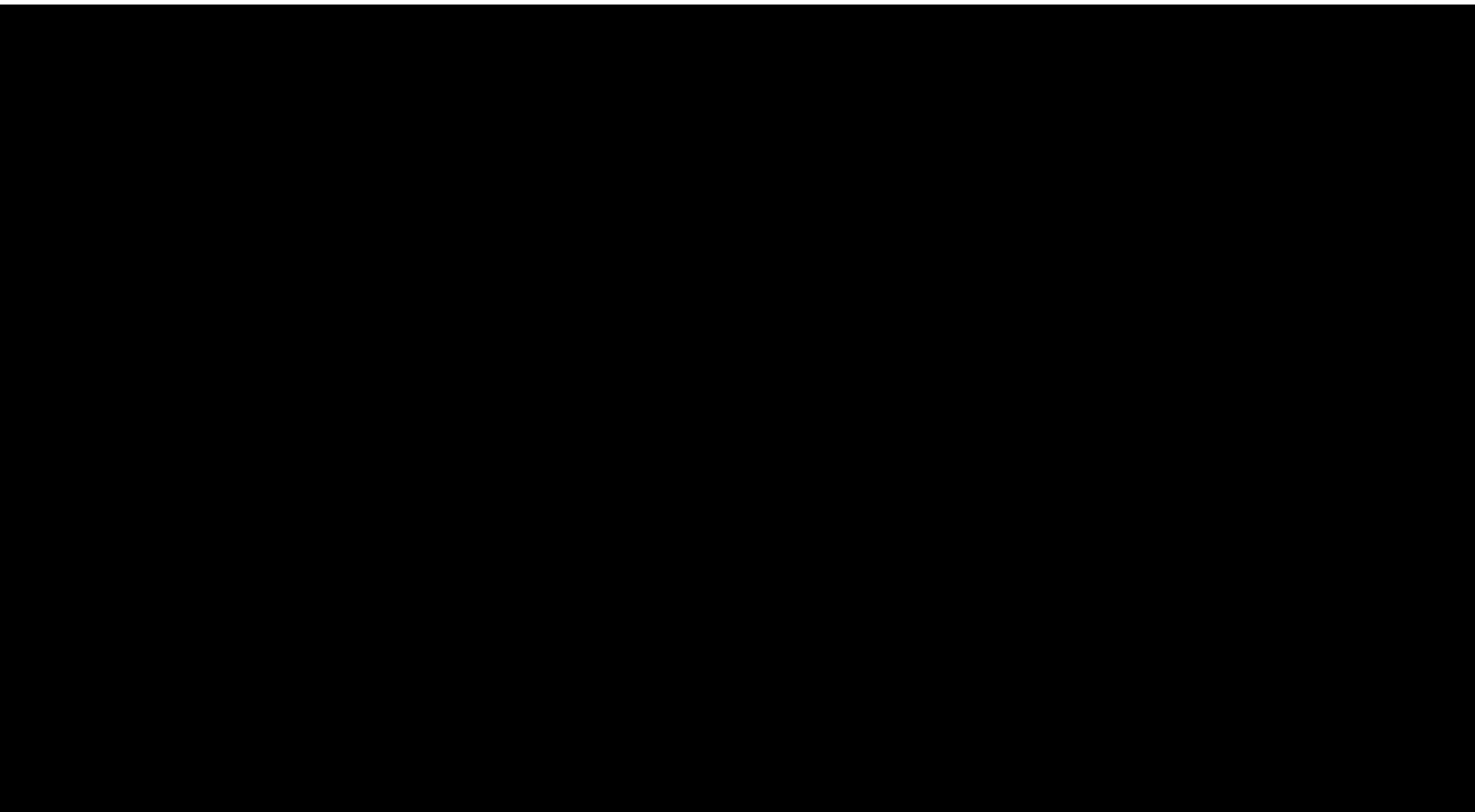

This dissertation is dedicated to Eto, Helen Elnatan and Kayla Harrington. Thank you for everything and believing in me.

Acknowledgements

The works presented here is a collection of my work done in the Agard lab. Chapter 1 of this thesis has been published at *eLife*(see Preface 1.1 for more details):

Elnatan, D., Betegon, M., Liu, Y., Ramelot, T., Kennedy, M. A. & Agard, D. A. Symmetry broken and rebroken during the ATP hydrolysis cycle of the mitochondrial Hsp90 TRAP1. *eLife* **6**, e25235 (July 2017)

The second chapter consists of work that I'm finishing up. It would not have been possible to do this without all of the wonderful people that helped me along the way. Ideas simply do not exist in a vacuum. I want to take this opportunity to thank them for their contributions in this thesis.

First and foremost, I'd like to thank David Agard for his guidance, (high-quality) intellectual input, and most importantly, his patience in being a mentor. Thank you for giving me the freedom to explore my scientific curiosities.

I'd like to give special thanks to my previous advisor prior to graduate school, Sean Burgess at University of California, Davis. Without her mentoring, support, and encouragement, I probably would not be in graduate school.

I would thank my thesis committee Geeta Narlikar and Jason Gestwicki for their guidance and support throughout my project. I feel really lucky that we can have Jason at UCSF and I am honored when he agreed to be in my thesis committee, just shortly after he moved his lab from Michigan. And for Geeta, I would like to thank her beyond the role as a thesis committee member. She helped me tremendously during my second-try for the BioReg exam. I would've floundered without her excellent mentorship. The Narlikar lab has always been a second home base here at UCSF, and have significantly shaped my growth as a scientist.

Laura Lavery deserves a very special thanks for taking me on as a rotation student in the Agard lab. Her exceptional drive and enthusiasm in science was inspiring. She practically taught me everything I know about molecular biology and biochemistry. I feel extremely lucky to have

been a part of her thesis work in mitochondrial Hsp90 (TRAP1), which paved the way for my own thesis work. I also want to thank James Partridge, a post-doc also working on TRAP1 at the time, for teaching me how to read between the lines of a protein purification protocol.

The Agard lab has always been a supportive environment for me. In particular, I'd like to thank Mariano Tabios and Joyce Ramponi for their patience in dealing with my mischiefs and being very helpful in times of distress. From the Hsp90 subgroup, I want to thank Timothy Street for teaching me how to work with tricky protein preps of Hsp90 clients and always willing to talk about models of how Hsp90 hydrolyzes ATP. I thank Elaine Kirschke for always being enthusiastic to discuss other molecular chaperones beyond Hsp90. I want to thank Kliment Verba, who taught me to appreciate everything mechanical and continue to inspire me for always being curious. I want to thank Miguel Betegon, my partner-in-crime for the work done in Chapter 1 of this thesis, for all of his contributions in making this work possible. I also appreciate his vigilance for keeping a nice clean lab bench. From the centrosome subgroup, I express my limitless gratitude to Andrew Lyon, who equally enjoys moving around math symbols on a piece of paper as much as I do. I'm deeply grateful for Rose citron, who taught me practical aspects of crystallography. This allowed me to eventually solve the crystal structure of the heterodimeric TRAP1.

From the Cooke lab, I want to thank Roger Cooke for his generosity in helping me with Electron Paramagnetic Resonance (EPR) experiments, and also for taking me on those fun sailing trips on the San Francisco bay. I want to thank Nariperson for helping me in all of the EPR experiments, all the delicious meals, and encouragements along the way.

As for my second home base, I want to thank the Geeta and the Narlikar lab members for making science much more fun and being so welcoming to me. I'm extremely lucky to have been involved in the heterochromatin work with Adam Larson. That experience really highlighted how fun doing science with your friend can be. I'm grateful for Coral Zhou for always being so positive and organizing all those chinese food lunches.

The UCSF community has been supportive and made doing science fun. I want to thank Muthuvel Arigovindan for showing me a glimpse of what it's like to do math for a real-world

problem in microscopy. I want to thank Bo Huang for letting me rotate in his lab and introduced me to the concept of 'compressed sensing'. Although brief, my interactions with these guys have empowered me, and they made me realize how much I love math and physics.

Abstract

Asymmetric mechanism of molecular chaperone Hsp90

By

Daniel Elnatan

Hsp90 is a highly conserved, ATP-dependent molecular chaperone that is essential for maintaining the functions of its client proteins. It has been estimated that about 10% of the proteome of a eukaryotic cell interacts with Hsp90. A large subset of this portion consists of protein kinases and steroid hormone receptors, putting Hsp90 as the master regulator of many essential cellular functions. The mechanism of how Hsp90 uses ATP hydrolysis to carry out its function remains unclear. Structural studies of Hsp90 revealed that Hsp90 is a V-shaped homodimer with each protomer composed of three well-folded domains: an ATP-binding N-terminal Domain (NTD), a Middle Domain (MD), and a C-terminal dimerization Domain (CTD). Efficient ATP hydrolysis by Hsp90 requires that the dimer forms a closed state where NTDs are dimerized, forming a closed ”clamp” conformation that is stabilized by ATP binding. The kinetics of forming this stably closed state is not driven by ATP binding, as there are other rate-limiting steps that need to occur within the protein to allow the NTDs to be dimerized. So how does Hsp90 actually use the energy from ATP to remodel its client protein? the focus of this thesis examines the other possibility of this happening during ATP hydrolysis. In the first chapter, I followed up an observation made by a previous graduate student Laura Lavery. She observed that the ATP-bound closed state of a mitochondrial Hsp90 (TRAP1) is asymmetric. The asymmetry is most prominent at the juncture between the MD:CTD interface—one protomer is buckled while the other remains straight, resembling the same conformation previously observed in the symmetric closed ”clamp” state. This buckling happens precisely where conserved binding sites have been mapped for client proteins. This suggests that if conformational changes were to occur due to ATP hydrolysis, subsequent rearrangements of the asymmetric MD:CTD interfaces back to the previously observed symmetric closed state

could be used to drive client protein remodeling. Using a combination of biophysical methods (crystallography, Double Electron-Electron Resonance (DEER), and FRET), we observed that TRAP1 hydrolyzes the 2 bound ATPs sequentially. The buckled protomer hydrolyzes the first ATP, which is then followed by a flip in the asymmetry (the buckled conformation becomes straight and vice versa, on each side), which primes the second ATP for hydrolysis by a buckled protomer. In this model, the MD:CTD interface is guaranteed to undergo remodeling with each ATP hydrolysis and would make efficient use of energy from ATP. The implications for this asymmetric ATP hydrolysis mechanism may also be relevant to other Hsp90s. While we have not observed any other asymmetric Hsp90 structures by itself, several functional Hsp90 complexes seen so far seem to have asymmetric composition/arrangements of their components. In the second chapter, we explore how TRAP1 ATPase activity can be modulated by different divalent cations as co-factors. Despite having two ATP binding sites, the ATPase activity of most Hsp90 homologs appears to be non-cooperative (each site behaves independently from one another). However, we saw that ATPase activity of TRAP1 can be cooperative in presence of calcium, and the activity in presence of magnesium appears to be bi-phasic, with higher activity at low ATP concentrations. This unique behavior of TRAP1 may yet be another adaptation of the Hsp90 machine that has evolved within the mitochondrial matrix environment. Using crystallography, we also discovered that calcium binds to the NTD of TRAP1 unlike previously observed chaperone/calcium/ATP complexes. While the exact biological role for this phenomena is not yet clear, these findings provide a clear molecular basis for the regulation of TRAP1 by calcium. Taken together, the work described in this thesis provide insights into the mechanism of ATP hydrolysis by Hsp90, and a potential role that TRAP1 plays in calcium/magnesium-regulated mitochondrial physiology.

Table of Contents

List of Figures

Chapter 1

Chapter 2

List of Tables

Chapter 1

Chapter 2

Chapter 1

Symmetry broken and rebroken during the ATP hydrolysis cycle of the mitochondrial Hsp90 TRAP1

1.1 Preface

The text of this chapter is a reprint of the material as it appears in *eLife* [14]. The corresponding author listed in this publication (David Agard) directed and supervised the research that forms the basis for the thesis. The work would not have been possible without the help of another graduate student in the lab, Miguel Betegon, who co-wrote the paper with me, in trying to figure out how TRAP1 uses energy from ATP hydrolysis. Miguel was able to obtain crystal structures of the zebrafish TRAP1 with ATP and directly watch ATP hydrolysis as it happens in the crystal over a period of months. The insight gained from his observation allowed us to infer the order of ATP hydrolysis by TRAP1, finally answering a big question that puzzled us since the original TRAP1 work by Laura Lavery. Our collaborators Mike Kennedy and Theresa Ramelot, at Miami University in Ohio, performed the DEER (Double Electron-Electron Resonance) experiments on my protein samples which motivated the big ideas for this work. My contribution to the manuscript is the rest of development and execution of biochemical assays, and a crystal structure of an engineered heterodimeric TRAP1 that culminate into the final model of TRAP1 cycle. I'm indebted to John Bruning, who collected the dataset for the one good heterodimeric TRAP1 crystal apart from about one-hundred poorly-diffracting ones I collected, which allowed me to finally solve the structure.

Crystal structures resulting from this work can be downloaded from the PDB (5TVW, 5TVX, 5TVU, and 5TTH).

1.2 Introduction

Heat-shock protein 90 (Hsp90) is a highly conserved ATP-dependent molecular chaperone. Although originally identified and named as part of the heat-shock response, Hsp90's many important roles in the general stress response, regulation of protein function, disease and evolution are now appreciated. Hsp90 physically interacts with ˜10% of the proteome[65], highlighting its ability to recognize a broad range of substrate 'client' proteins, having diverse functions, sequences, structures, and sizes. Although Hsp90 can function as a canonical chaperone and promote protein folding by suppressing aggregation[25, 61], it is unique in that it also plays an active role in regulating the activities of a large subset of the proteome, including many proteins involved in signal transduction such as kinases and hormone receptors, thus supporting normal cellular functions. This essential function of Hsp90 is intimately tied to its ATPase activity, and mutations that either enhance or suppress this activity compromise cell viability[39, 40]. Conversely, deregulation of cellular Hsp90 levels helps support uncontrolled growth in many human cancers making Hsp90 an important pharmacological target[60].

Hsp90 is a V-shaped homodimer, with each protomer consisting of three major domains: a C-terminal dimerization domain (CTD); a middle domain (MD), which has been linked to client binding; and an N-terminal ATPase domain (NTD). The Hsp90 NTD and the upper part of the MD confer membership to the GHKL (DNA Gyrase, Hsp90, Histidine Kinases, MutL mismatch repair protein) family of ATP-powered molecular machines.

In the apo state, Hsp90 is highly dynamic and can sample a range of conformations from a highly extended to a more compact state, potentially accommodating interactions with a diverse set of client structures and sizes[26]. Large conformational changes are also coupled to nucleotide binding: ATP binding stabilizes a closed state where both NTDs are dimerized, forming the cat-

alytically active state, whereas ADP binding favors a transiently formed compact state[54]. Such structural studies have suggested an ATPase cycle of closure, hydrolysis and reopening.

Most higher eukaryotic cells possess four Hsp90 homologs: two cytosolic isoforms, one of which is constitutively expressed while the other is induced by heat shock and stress (Hsp90b and Hsp90a, respectively), one localized to the endoplasmic reticulum (Grp94) and one localized to the mitochondria (TRAP1). Despite some sequence divergence and a few insertions/deletions decorating the globular domains, the structures of all Hsp90 homologs remain conserved, suggesting a fundamental mechanism that adapted to different cellular environments. Indeed, a survey of conformational states in bacterial, yeast, and human Hsp90 revealed species-specific tuning of conformational equilibria and ATPase rates[56]. In general, reaching the NTD-dimerized closed state is rate limiting for ATP hydrolysis. In the case of TRAP1, the formation of this closed state is further regulated by a temperature-sensitive kinetic barrier imparted by an extra N-terminal extension[42]. For eukaryotic cytosolic Hsp90s, binding of co-chaperones can stabilize particular conformational states and modulate ATPase activity[13, 47, 55].

Despite the wealth of information regarding Hsp90 dynamics, little is known about how the energy of ATP hydrolysis is coupled to client protein remodeling. The current model focuses attention on the ATP-induced large conformational change going from a wide-open V-shape to the NTDdimerized closed state, whereas conversion to the compact ADP state would displace the bound client, followed by reopening to reset the chaperone. However, given that these conformational states are roughly isoenergetic and that ATP binding only marginally stabilizes the closed state[35, 56], this model does not provide a clear connection between utilization of energy from ATP hydrolysis and client remodeling. A recent crystal structure of AMPPNP-bound zebrafish TRAP1 (zTRAP1) in a closed state [27] revealed a novel conformational asymmetry between the protomers, most pronounced at the MD:CTD interfaces where one has 2.5-fold more buried surface area than the other (400 Å vs. 1000 Å). One of the protomer arms is buckled while the other remains straight, nearly identical to the previously observed conformation in p23-bound yeast Hsp90 (yHsp90) closed state [2]. Notably, the previously determined client-binding site[17, 58] located at

the MD:CTD interface is maximally affected by the protomer asymmetry.

Using TRAP1 as a model system for Hsp90, here we investigate how ATP hydrolysis is coupled to its conformational asymmetry and propose a model connecting it to client remodeling. We examine whether ATP hydrolysis in TRAP1 is sequential, what the order of hydrolysis events is, and how the asymmetry is coupled to the nucleotide states along the ATPase cycle. By covalently linking TRAP1 monomers, we created homogeneous populations of obligate heterodimers having one hydrolysis-dead protomer, and determined that TRAP1 must undergo ATP hydrolysis in both protomers to efficiently progress through the cycle. Crystal structures of WT TRAP1 closed with ATP in the absence of Mg^{2+} showed that the buckled protomer hydrolyzes ATP more rapidly than the straight one. Microsecond-long molecular dynamics simulations reveal differences in water dynamics within the nucleotide-binding pocket of each protomer, highlighting distinct environments surrounding the ATP that may establish differences in hydrolysis rates. Pulsed electron paramagnetic resonance (EPR) distance measurements using dipolar electron-electron resonance (DEER) methods revealed that, in solution, a TRAP1 mutant mimicking the hemi-hydrolyzed (ATP/ADP) state adopts a uniform conformation distinct from the stochastic mixture seen in WT. In this heterodimer, the protomer containing ATP is buckled while the protomer containing the ADP-mimicking mutation is straight. Integrating this data, we propose a revised model of the TRAP1 ATP-driven cycle where the two hydrolysis events are sequential and deterministic, with the buckled protomer being most competent for ATPase hydrolysis, followed by a flip in the MD:CTD asymmetry to position the opposite protomer in the buckled conformation, promoting hydrolysis of the second ATP and allowing TRAP1 to proceed through the cycle.

1.3 Results

Two ATP hydrolyses are required by TRAP1 to progress through its ATPase cycle

Previous studies on various Hsp90s show that their ATPase activities follow simple, non-cooperative kinetics despite having two ATP-binding sites[11, 16, 34, 49]. Consistent with these observations, the activity of the wild-type ATPase domain is unaffected by whether its partner carries a mutation that does not bind ATP or one that does not hydrolyze ATP[8, 48]. Such heterodimeric studies are possible because Hsp90 dimers dynamically exchange within minutes[20, 48]. Simply mixing wild-type and mutant proteins creates a mixture of dimer species (wild-type + heterodimer + mutant) at equilibrium. Using this approach, we looked at human TRAP1 (hTRAP1) ATPase activity by mixing wild-type and a point mutant (E115A) that impairs ATP hydrolysis, but not ATP binding[40] at different ratios. In contrast to previous studies, the activities of these TRAP1 mixtures are lower than what is expected if the two ATPase domains were to act independently (Figure 1.1A), suggesting TRAP1 requires that both bound ATPs be hydrolyzed in its ATPase cycle. Since these experiments were done under steady-state conditions, the decreased activity of heterodimers can be due to either an impaired ability to form the closed state or an impaired ability to exit the closed state, thus changing the rate-limiting step.

To distinguish between these models, one can form heterodimers by mixing and use FRET to directly probe the conformation of the dimer[20]. However, a significant drawback is that the resulting mixture of dimer species complicates further biochemical or especially structural analyses. To allow precise targeting of protomer-specific mutations and produce a homogeneous population of heterodimers without dimer exchange, a covalently bound heterodimeric hTRAP1 was engineered using SpyCatcher/SpyTag[64] appended after the CTD dimerization domain. Similar to our previous studies[42], we can efficiently monitor TRAP1 closure by attaching FRET probes to cysteines engineered into the NTD (E140C) and MD (K413C) of a cysteine-free chaperone

(Figure 1.1B). Using the covalent heterodimers, the E115A mutation was introduced to one of the protomers. Appropriate functionality was confirmed by observing that only half of the bound ATP was hydrolyzed under single-turnover conditions (Figure 1.1C). Since dimer closure is required to hydrolyze ATP, this rules out the model where the heterodimer cannot form the closed state. Furthermore, it suggests that the impaired steady-state ATPase of the dimer may be due to an inability to exit the closed state. If true, this would lead to a build up of the closed state under multiple-turnover conditions that can be monitored by FRET (high FRET), whereas constant turnover of the wild-type enzyme would maintain a low FRET signal. Indeed, this is just what is observed upon addition of 2 mM ATP/MgCl2 to either wild-type or +/E115A TRAP1 (Figure 1.1D). The buildup rate of the heterodimer (0.16 min-1) is comparable to the steady-state ATP turnover rate of the cysteine-free wild-type (0.19 min-1, Figure S1.2), indicating that having only one active ATP site does not affect the kinetics of forming the closed state. Since the closure rate of the +/E115A construct is not affected and dimer closure precedes ATP hydrolysis, the reduced steady-state ATPase rate must be due to a slower process that happens after the dimer is closed.

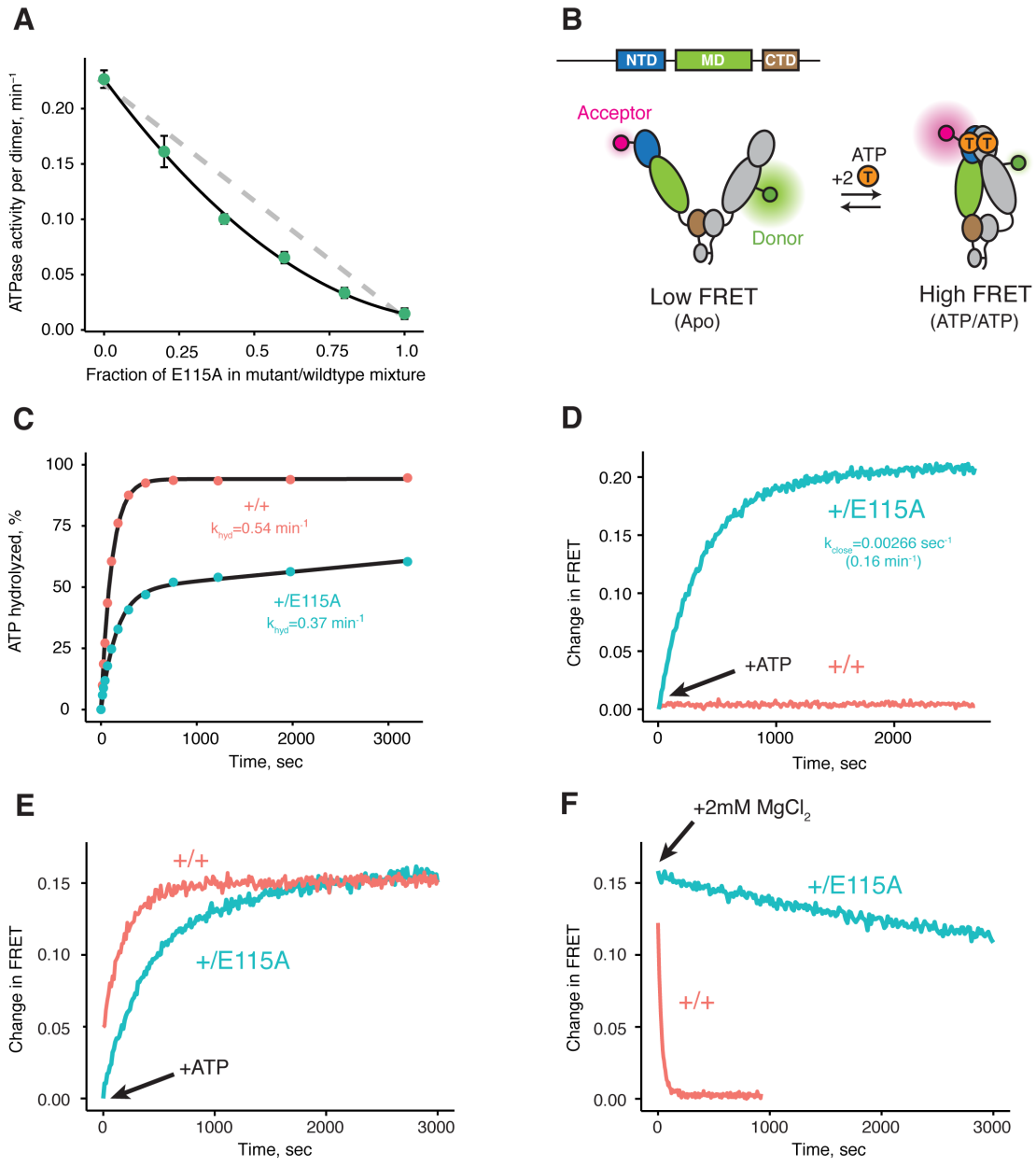

Figure 1.1: Both ATPs need to be hydrolyzed for efficient cycling. **A**) Steady-state ATPase assay with constant dimer concentration and varying ratios of wild-type and catalytically-dead E115A mutant shows that ATP hydrolysis by each protomer is not independent. Each point and error bar are one standard deviation and averaged from triplicate experiments. Black line is a fit to a binomial distribution of wild-type:mutant:heterodimer, solved for only the heterodimeric activity. The gray dashed line shows the expected activity for independent ATP hydrolysis. (**B**) Covalently linked heterodimers for the FRET assay with fluorescent labels on the NTD and MD (E140C, K413C respectively). (**C**) Single-turnover ATPase kinetics of wild-type (+/+, red) and heterodimeric, hemi-hydrolyzing (+/E115A, blue), show activity of the remaining site is not compromised. Black curves are exponential fits with an additional linear term to account for a slow steady-state activity in the

(**Figure 1.1**, *continued*) +/E115A. (**D**) FRET assay looking at build up of closed state (high FRET) in the +/ E115A heterodimer (+/E115A, blue) and wild-type (+/+, red) in presence of $MgCl_2$ to allow ATP turnover. The +/E115A data were fit to an exponential with the indicated rate, k_{close}. (**E**) FRET assay showing closed state build up in both +/+ (red) and +/E115A (blue) heterodimers after addition of 2 mM ATP in absence of $MgCl_2$. (**F**) Addition of excess MgCl2 triggers efficient dimer reopening, as measured by FRET, in +/+ (red) but not +/E115A (blue) heterodimers in reactions pre-incubated with ATP without Mg^{2+}.

To directly test the ability of the hemi-hydrolyzed dimer to exit the closed state, a FRET experiment was designed to look at the kinetics of dimer opening after ATP hydrolysis starting from a synchronized closed state population. This is possible because TRAP1 accumulates the closed state upon addition of ATP in absence of Mg^{2+} (Figure 1.1E), whereupon hydrolysis can be initiated by addition of excess $MgCl_2$[42]. If hydrolysis of both bound ATPs is required to reset TRAP1 back to an open state, then the hemi-hydrolyzing mutant should have an impaired re-opening rate after $MgCl_2$ is added. Indeed, a very slow re-opening rate is observed for the +/E115A heterodimers whereas the wild-type protein rapidly returns to low FRET baseline (Figure 1.1F). These observations strongly support a model where two ATP hydrolyses are required for TRAP1 to progress efficiently through its ATPase cycle.

Crystallographic evidence of sequential and deterministic ATP hydrolysis in TRAP1

The observed accumulation of TRAP1 closed state upon addition of ATP in the absence of Mg^{2+} appears to be specific to the mitochondrial homolog, as bacterial Hsp90 (bHsp90) and yHsp90 don't exhibit this behavior and remain in the open state (data not shown). To characterize this unique state and, through it, gain insight into the TRAP1 ATPase cycle, we crystallized zebrafish TRAP1 (zTRAP1) closed with ATP in the absence of Mg^{2+} with an excess of EDTA. An initial crystal, collected 3 days after setting crystal trays, diffracted to 2.5 Å and was solved using molecular replacement with the previously published TRAP1 structure closed with AMPPNP[27] (PDB:4IPE). The refined model showed no major conformational differences with any of the previously published

full-length TRAP1 structures closed with non-hydrolyzable nucleotides (Figure 1.2A). The same pronounced asymmetry (one straight protomer and one buckled protomer) was clearly observed. However, differences exist in the ATP binding pocket: as expected, the Mg^{2+} electron density previously observed contacting the nucleotide phosphates is missing and, surprisingly, while the straight protomer contained a mostly intact ATP, the buckled protomer had only weak density for the γ-phosphate (Figure 1.2B, Day 3). This clearly indicated that the buckled protomer preferentially hydrolyzes ATP, but does not inform on whether hydrolysis occurred before or after crystallization.

To differentiate between these possibilities, we took advantage of the fact that our crystals grow overnight, allowing collection and freezing of crystals every 24 hours for a time-resolved experiment. After screening crystals from multiple time points for diffraction quality, two additional datasets were collected (1-day and 53-day old crystals), solved and refined through the same methods to resolutions of 3.5 Å and 2.2 Å respectively. Similar to the three-day old crystal, no significant conformational differences were observed and no Mg^{2+} ion density was present in the ATP binding pocket. However, electron densities for the ATP molecules showed a monotonic progression from an ATP-ATP structure (one day old crystal) through an ATP-ADP intermediate (3-day old crystal) to an ADP-ADP structure (53-day old crystal) (Figure 1.2B), clearly demonstrating that hydrolysis is occurring in the crystal. This result leads to a model in which TRAP1 hydrolysis events are sequential and deterministic, with the buckled protomer conformation being catalytically favorable and hydrolyzing first. At least in the context of the crystal lattice, no major conformational rearrangements of the symmetry are linked to the first ATP hydrolysis.

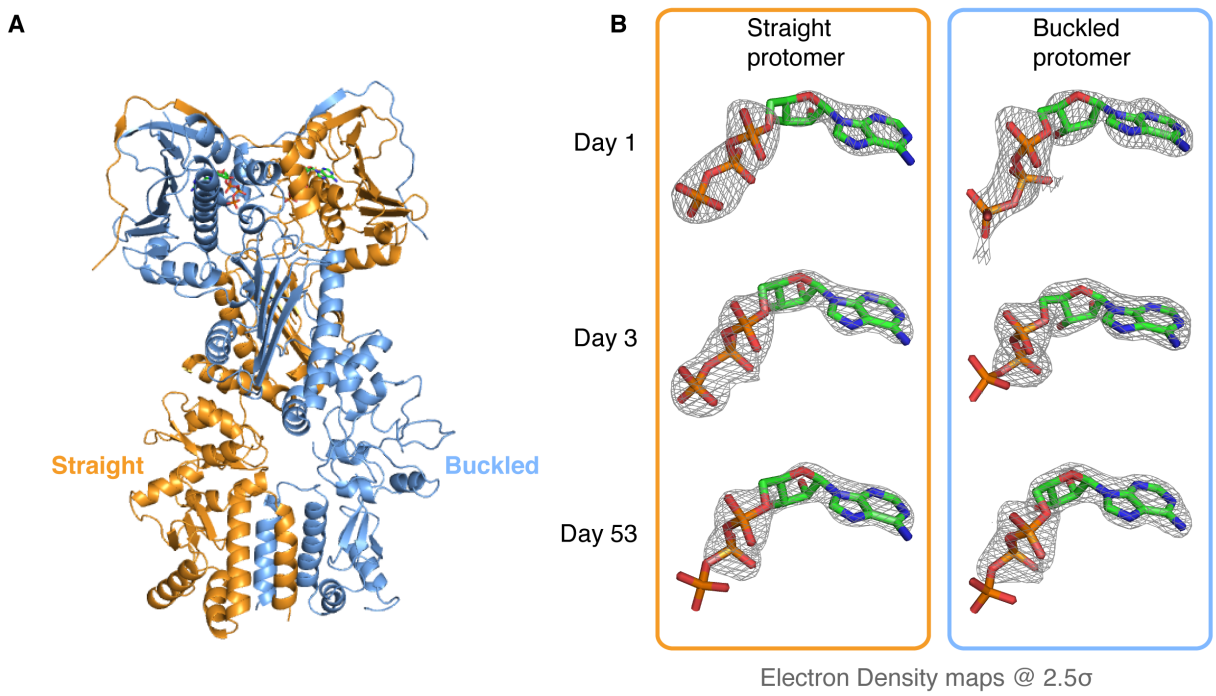

Figure 1.2: Kinetic crystallography indicates that the buckled arm hydrolyzes ATP first. (**A**) 2.3 Å crystal structure of zTRAP1 closed with ATP obtained from a 3-day-old crystal showing minimal conformational changes without Mg^{2+}. Buckled protomer is in blue and straight protomer is in orange. (**B**) ATP electron density maps for the buckled and straight protomers from crystals of different ages showing the evolution of in-crystal hydrolysis.

TRAP1 hydrolyzes ATP in solution in absence of Magnesium

The fortuitous crystallographic observation of two different ATP hydrolysis rates in the closed state indicates that TRAP1 has the capacity for ATP hydrolysis in the absence of Mg^{2+}, albeit slowly. To exclude the possibility that this was somehow unique to the crystal, we needed an extremely sensitive solution assay that could detect TRAP1 ATPase activity in the absence of Mg^{2+} – a level that could be near the rate of spontaneous ATP hydrolysis. A sensitive fluorescent phosphate sensor[6] was chosen for a simple kinetic assay as done by McLaughlin et al. with human Hsp90 (hHsp90). While ideally this would be done using zTRAP1 to match the crystallography, its much weaker Km would require an order of magnitude higher ATP concentration to trap the closed state

than the human homolog (Figure 1.3A). This would be problematic as it introduces a high free phosphate background from ATP alone. Instead, human TRAP1 was used to detect ATP hydrolysis in solution with 500 μM of ATP in the presence of excess EDTA. At this ATP concentration, there is no significant amount of apo state by size exclusion chromatography (Figure 1.3B) and the ATP titration by FRET estimates at least 80% closed state (Figure 1.3A).

Under this condition, a low but significant ATPase activity is detected in solution (Figure 1.3C). This ATPase is specific to TRAP1, since the rate of hydrolysis scales with TRAP1 concentration (Figure 1.3D), and it can be inhibited by the addition of Radicicol (Figure 1.3C), a potent ATPase inhibitor for Hsp90[28]. From this experiment, the spontaneous and TRAP1-catalyzed (Mg^{2+}-free) ATP hydrolysis rates are 0.00155 and 0.5808 per hour (per active site), respectively. Spontaneous hydrolysis would take 62 days whereas the protein-catalyzed hydrolysis would take 4 hours to hydrolyze 90% of the initial ATP concentration. Although we do not have time points between 1, 3, and 53 days for the crystallography, within an order of magnitude, the solution rates roughly correspond to what we see in the crystal. After three days, ATP is fully hydrolyzed by the buckled protomer while ATP remains intact in the straight protomer. Under the same experimental conditions, the rate of dimer closure is an order of magnitude faster (6.95 per hour) than the observed hydrolysis rates(Figure S1.3). Since dimer closure is no longer the slowest step in hydrolysis, it's likely that in absence of Mg^{2+}, hydrolysis of the first ATP by the buckled protomer is now the rate-limiting step.

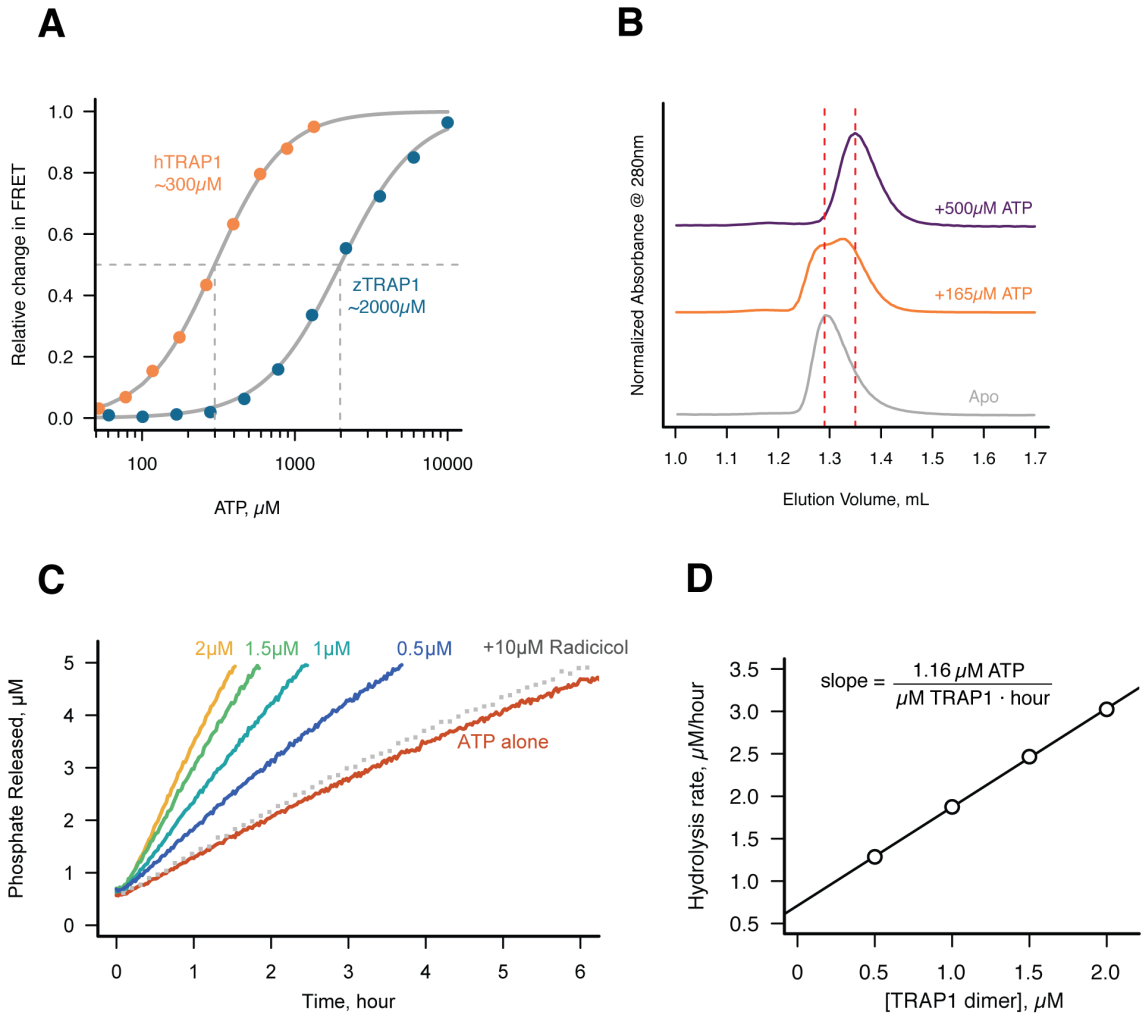

Figure 1.3: Without Mg^{2+} hTRAP1 adopts the closed state and slowly hydrolyzes ATP in solution. (**A**) Equilibrium titration of closure in response to ATP in presence of excess EDTA hTRAP1 (orange) and zTRAP1 (dark blue) using FRET. The indicated half-max concentrations are obtained from fits to the Hill equation (gray lines). (**B**) Size-exclusion chromatography of cysteine-free TRAP1 under apo (gray), and after 1.5 hr incubation at 30 °C with 165 μM ATP (partial closure, orange), and 500 μM ATP (full closure, purple). Red dashed lines are guides for apo and closed state peak positions. (**C**) Ultra sensitive assay of ATP hydrolysis using fluorescent phosphate-release assay with PBP-MDCC with ATP alone (red) and varying dimer concentrations of cysteine-free TRAP1, and 2 μM TRAP1 + 10 μM radicicol (gray dotted line). (**D**) Initial rates from phosphate-release kinetics plotted against TRAP1 dimer concentration confirming that the rate above baseline is TRAP1 dependent. The ATPase hydrolysis rate per TRAP1 dimer is 1.16 μM ATP · μM TRAP1^{-1} hr^{-1}.

Asymmetric water dynamics near ATP γ-Phosphate between protomers

To further explore the structural origins of the differential rates of ATP hydrolysis by the two protomers, we performed microsecond all-atom molecular dynamics simulations based on the crystal structure of the asymmetric zTrap1 dimer (PDB ID: 4IYN). We focused on dynamics as no significant differences in the coordinates of the two active sites were observed in the crystal structures. As part of the straight ATP binding pocket lid was disordered in the crystal structure, the ATP lid regions of both protomers were modeled to be identical and ordered. The ATP analog ADP-AlF4 in the crystal structure was replaced with ATP in the presence of Mg^{2+}. The simulations were carried out with explicit water at two different temperatures (310 K and 360 K). The high temperature was used to enhance the conformational sampling.

The structures are intact throughout the simulations at both temperatures and exhibit a high degree of flexibility at the microsecond time scale. To investigate a possible mechanism of how the differential ATP hydrolysis is established, we focused on the environment surrounding the ATP. We monitored the numbers of water molecules within a 5 Å radius of the ATP β- and γ-phosphate along the trajectories, sampled every 3 ns.

On average, the ATP γ-phosphate in the buckled protomer has fewer water molecules in proximity than the one in the straight protomer (Figure 1.4A). At higher temperature, the same trend is maintained despite a larger overlap between the distributions (Figure S1.4A). This was unexpected given that both of the nucleotide binding pockets appear to be essentially identical. The average RMSD between the N-terminal domain of the two protomers is 1.74 Å. The different water dynamics likely arises from differential dynamics of the two protomers.

In addition to the different water occupancy, the most striking difference between protomers observed in the simulations are the water dynamics near the two ATP β- and γ-phosphates. Excluding the Mg^{2+} coordination waters (Figure 1.4B,C), most of the waters spend only a few nanoseconds (Figure 1.4B, green) in the buckled protomer. In contrast, in the straight protomer, there are longer-lived waters positioned between E130 and the γ-phosphate (Figure 1.4C, red vs 4B, green) and also

more waters positioned above E130 (Figure 1.4C, white). This trend is also observed at high temperature (Figure S1.4B,C). While the precise mechanism is still unclear, this asymmetry in water occupancy and dynamics between two protomers likely correlates with the observed preferential hydrolysis of the buckled protomer ATP observed in the time-resolved X-ray crystallography.

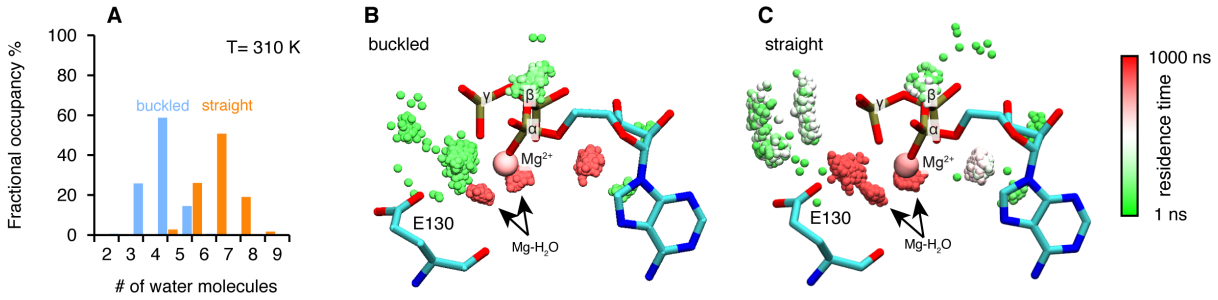

Figure 1.4: Microsecond all-atom molecular dynamics simulations of zTrap1 reveal asymmetric water dynamics near the ATP γ-phosphate. (**A**) Histogram of water molecules counted near the ATP β- and γ-phosphates ($<$5 Å) throughout the simulation (each frame is three ns) in the buckled protomer (blue) and the straight protomer (orange) at T = 310 K. (**B**) and (**C**) Fractional residence time of each individual water molecule in the ATP-binding pocket for the buckled and straight protomers at T = 310 K, showing significant differences in solvation near the E130. Only the oxygen of water molecules near the ATP β- and γ-phosphates ($<$5 Å) are shown. Points are accumulated from all frames along the trajectory after aligning the system based on the ATP. Black arrows point to the persistent magnesium-coordinated water molecules, Mg-H_2O, which are conserved for the two conformers. Water molecules were colored based on their residence time as indicated by the color bar.

Loss of the γ-Phosphate contact determines MD:CTD conformation in the ATP/ADP state

ATP analogs have been successfully used to capture pre- and post-hydrolysis transition intermediate conformational states of several ATPases providing insights into their mechanisms[7, 15, 63]. In contrast, previous TRAP1 experiments with these analogs resulted in similar asymmetric structures with no obvious conformational differences. In our time-resolved crystallography experiments, the solved structures remain in essentially the same conformation despite having gone

through a full conversion from two ATPs to two ADPs. Because crystallographic packing likely prevents any significant conformational changes that might occur after the first ATP hydrolysis, DEER[41] was again the optimal choice for directly probing the solution MD:CTD conformation of hTRAP1 in the hemi-hydrolyzed (ATP/ADP) state. The challenge is then to capture a stable ATP/ADP hybrid state.

To generate an ADP-state in only one protomer, we make use of the observation that the MD-Arg (R402 in hTRAP1), the only residue in Hsp90 that contacts the γ-phosphate, acts as an ATP sensor[9] and mutating this residue would effectively mimic the ADP state. Using the SpyCatcher/SpyTag heterodimer, we introduced a point mutant (R402A) to break the γ-phosphate contact in only one protomer. This heterodimeric construct (+/R402A) can form the closed state upon incubation with the ATP analog ADP-BeF (Figure S1.5) and has minimally perturbed (2-fold increase) ATPase activity (Figure S1.2). A cysteine-free version of this heterodimer was used for site-directed spin labeling at the MD (K439C) and CTD (D684C). These positions optimally report on unique MD:CTD distances within each protomer. By measuring the distance between these probes via DEER, one can distinguish between a buckled or straight conformation of the labeled protomer in the closed state[27]. As expected for the wild-type heterodimer, two peaks were observed centered at about 22 Å and 41 Å with roughly equal proportions (Figure 1.5A). This is close to the 50:50 probability of a protomer randomly adopting either conformation in an asymmetric closed state. Although the observed distances do not exactly match the corresponding values from the crystal structures, they are well within measurement uncertainties when the maleimide linker (˜8 Å) and broad distribution of distances are taken into account. Placing this spin-label pair on a protomer carrying the R402A mutation (+/R402A cis) or across from that mutant protomer (+/R402A trans) can independently report on both MD:CTD conformations of the hemi-hydrolyzed dimer in the closed state.

If TRAP1 adopts a symmetric closed state after losing one γ-phosphate contact, a single distance should be observed irrespective of spin-label placement in the hemi-hydrolyzed state. Instead, two different distances were observed depending on the placement of the spin-labels with

respect to the R402A mutation. Protomers with an intact γ-phosphate contact adopt mostly a 22 Å MD:CTD distance - consistent with the buckled conformation (Figure 1.5B), whereas spin-labeled protomers lacking the γ-phosphate contact exhibit a major peak at 41 Å - consistent with the straight conformation (Figure 1.5C). Our interpretation that these distances faithfully report on the MD:CTD conformations rely on assumptions that the spin-labels, the R417A mutation, or the SpyCatcher fusion did not introduce unintended perturbations.

To address this concern, we crystallized an equivalent heterodimeric construct of zTRAP1 (+/R417A in zebrafish sequence numbering) in the presence of ADP-BeF. The heterodimeric crystal diffracted to 3.2 Å and was solved with molecular replacement using the published model of ADP-BeF-bound zTRAP1[27] (PDB:4J0B) and a SpyCatcher-SpyTag complex[30] (PDB:4MLS). As predicted from the DEER results, the heterodimer adopts an essentially identical asymmetric closed state (Figure 1.5D), and the C-terminal-fused SpyCatcher-SpyTag complex packs against its symmetry mate in the opposing dimer (Figure S1.6). The structure shows that the R417A mutation does not perturb the overall closed state. To avoid model bias, the dataset was refined starting with alanines replacing arginines at positions 417 on both protomers. The Fo-Fc difference map (Figure 1.5D, insets) show strong positive density for the arginine only on the buckled protomer (ATP state), while the R417A mutation is on the straight protomer (ADP state). This is completely consistent with the interprobe distances measured in the DEER experiments correctly representing the buckled and straight protomer conformations. Altogether, this demonstrates that the loss of the γ-phosphate contact within the closed dimer is a strong determinant of the corresponding protomer conformation. Thus, the first ATP hydrolysis directly alters dimer asymmetry upon phosphate release.

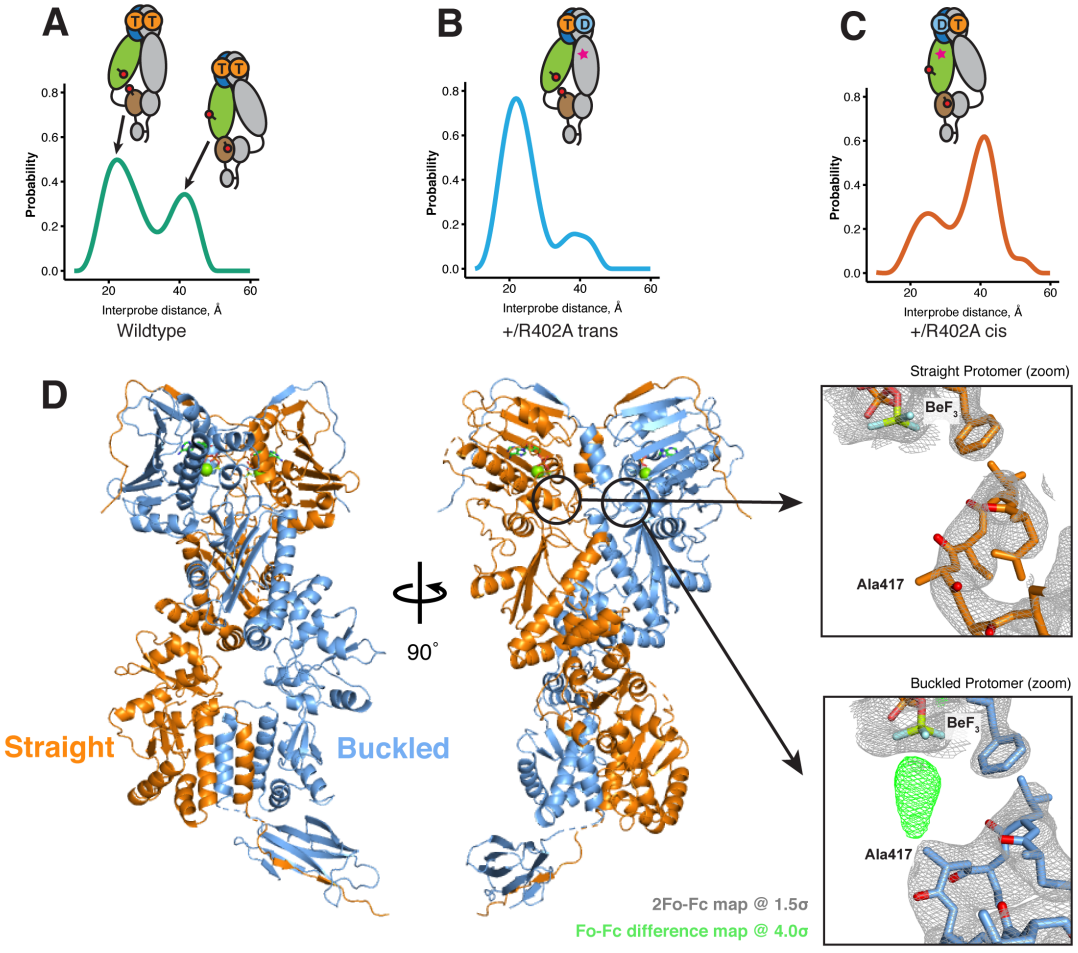

Figure 1.5: The asymmetry is flipped in the ATP/ADP state as revealed by DEER on hemi-hydrolyzed (ATP/ADP) heterodimers. The cartoons depict hTRAP1 heterodimers (one protomer colored by domains and the other in gray; NTD, blue; MD, green; CTD, brown) with spin-labels (red circles) and the relevant nucleotide state (D or T, for ADP or ATP, respectively) as well as the R402A mutation (ADP state mimic; magenta star). The SpyCatcher/SpyTag is shown attached to the CTD tails. (**A**) +/+heterodimers (green line) partition roughly equally between the buckled (left, 22 Å) and straight (right, 41 Å) conformations. (**B**) Spin-labels on the opposite (*trans*) protomer of +/R402A heterodimers (blue line) show that nearly all molecules are buckled on the ATP arm. (**C**) +/R402A heterodimers (orange line) carrying spin-labels on the same (*cis*) protomer as the R402A mutation, showing that the protomer prefers the straight conformation. (**D**) Crystal structure of +/R417A heterodimeric zTrap1 with the SpyCatcher-SpyTag fusion in the asymmetric closed state showing buckled (blue) and straight (orange) protomers. The dashed line indicates disordered residues. Insets show that the g- phosphate-sensing R417 is only present on the buckled arm. Phases come from a model having Ala on both protomers. $2F_o - F_c$ density (gray mesh) and $F_o - F_c$ difference map (green mesh) around the position of the asymmetric R417A mutation. Strong positive density (green mesh) on the difference map is observed only at the buckled protomer.

1.4 Discussion

Previous equilibrium Hsp90 structural studies have provided a picture of a dynamic molecular machine whose conformational ensemble, well described by rigid-body motions of its globular domains, is differentially tuned, but not exclusively determined by nucleotide binding. While ATP-binding has a clear role in stabilizing the NTD-dimerized closed state — depicted clearly by closed states of yHsp90[2], zTRAP1[27], and hHsp90[59] — the role of ATP hydrolysis in Hsp90's conformational cycle remains unclear. In this study, we present evidence for a sequential, deterministic hydrolysis of the two ATPs within the mitochondrial Hsp90 (TRAP1) dimer. Each step of hydrolysis drives conformational changes at the client binding site located at the juncture between the middle and C-terminal domains. We discuss below how this provides a new framework for understanding the mechanism of ATP-dependent client remodeling by Hsp90.

Mechanism of conformational coupling to sequential ATP hydrolysis

Earlier TRAP1 studies had shown how the strain of closing results in a markedly asymmetric (straight:buckled) two-ATP (ATP/ATP) closed state both in the crystal and in solution[27]. Unlike the stochastic picture that emerged from equilibrium structural studies[26, 35, 56] here we show that hydrolysis of both ATPs is required for efficient reopening. Thus once closed, kinetic rather than thermodynamic processes govern progression through the conformational cycle. Given this observation, we focused on whether the order of ATP hydrolysis depends upon the asymmetry and on what happens after the first ATP is hydrolyzed.

To facilitate this work, covalent heterodimers were efficiently created using C-terminal fusions with SpyCatcher and SpyTag[64]. Also critical, was the ability to close TRAP1 with ATP but in the absence of Mg^{2+}, allowing the normally rate-limiting closure step to be bypassed, thereby synchronizing all molecules in a closed ATP/ATP state. The fortuitous ability of the Mg^{2+}-free closed state to be crystallized with ATP, allowed the slow hydrolysis process to be examined crystallographically using crystals of different ages – revealing that the buckled protomer hydrolyzes

ATP first while the straight protomer is still bound to an intact ATP. Concerned that the slow hydrolysis seen in the crystal could be an artifact of packing effects on the ATP lid, quantitative kinetics using a highly sensitive assay for phosphate release confirmed that in the absence of Mg^{2+}, ATP hydrolysis does occur slowly in solution.

What happens structurally after the first ATP is hydrolyzed? Unfortunately, beyond small perturbations, the crystal lattice blocks significant conformational rearrangements, even after weeks when both ATPs have been hydrolyzed. To resolve this, we used DEER measurements on heterodimers engineered to mimic the mixed ADP:ATP state in solution. In the ATP:ATP state, the labeled protomers adopt roughly an equal mixture of the two conformers, due to the random buckling on transition to the highly strained closed state. By contrast, after the first ATP hydrolysis, essentially all the molecules are in a defined state with the ADP protomer being straight and the ATP protomer buckled.

Combined, these results indicate that hydrolysis of the first ATP must alter the conformational asymmetry in all molecules such that the ADP containing protomer straightens while the remaining ATP protomer adopts the buckled, catalytically favorable conformation. Including our observation that reopening only efficiently occurs from the ADP:ADP state leads to the proposed conformational cycle revealing how ATP hydrolysis can potentially perform work to remodel a bound client protein (Figure 1.6).

(i) Binding ATP leads to stabilization of a strained, high-energy closed state[27, 42]. (ii) The buckled protomer preferentially hydrolyzes ATP, transiently producing a buckled ADP state. (iii) The asymmetry flips so that the ATP protomer is now buckled, setting it up for hydrolysis. (iv) The second ATP is hydrolyzed, leading to reopening, fully relieving strain. While this work was done with the mitochondrial Hsp90 ortholog, the proposed sequential hydrolysis mechanism also explain the lack of ATPase cooperativity observed in other Hsp90s[16, 49].

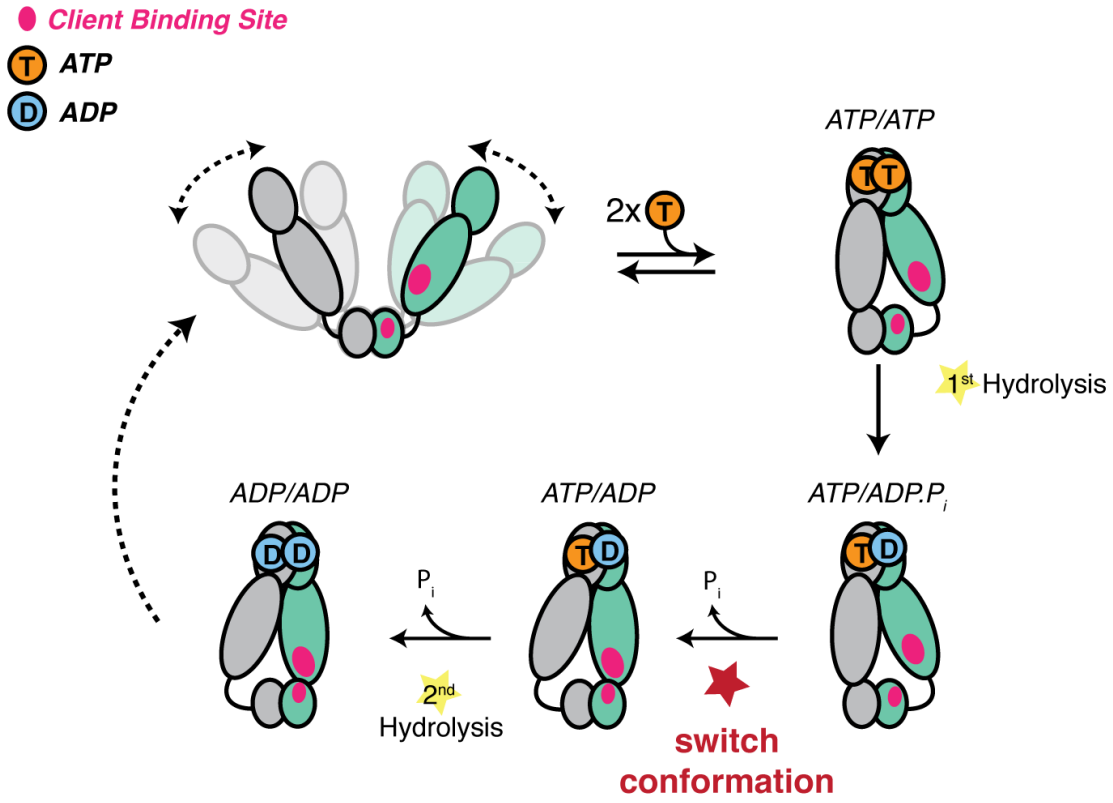

Figure 1.6: Revised model of the TRAP1 ATPase cycle showing the obligatory sequential hydrolysis and conformational switching. The protomers are colored teal and gray. The dynamic apo state (upper left) binds two ATPs, which stabilize a strained asymmetric NTD-dimerized closed state. Within this closed state, ATP is hydrolyzed first by the buckled protomer. Release of P_i likely drives the observed conformational switch of the straight protomer (ATP) to a buckled conformation, while the previously buckled protomer (now ADP), straightens. Concomitant with the flip, the client-binding sites (magenta ellipses) are rearranged, to facilitate client remodeling. Now in a buckled conformation, the second ATP is set up to be hydrolyzed. Finally, the ADP/ADP dimer re-opens, releasing nucleotides and resetting TRAP1 to the apo state.

A model for Hsp90 client maturation mechanism

Although Hsp90 has been studied for over 30 years and its importance in many key cellular processes established, the mechanism by which it matures a large set of diverse clients remains uncertain. This is partly due to Hsp90 preferentially interacting with intrinsically unstable proteins,

which has hampered in vitro studies of the chaperone in the context of these clients. In the absence of client proteins, Hsp90 cycles between a wide-open V-shaped apo state and a more compact closed state. In principle, rearrangements of hydrophobic residues accompanying the large conformational change (open-to-closed) could be used to remodel client protein, leading to a molecular "clamp" model[44]. However, we note that constricting the large open-to-close transition, as done by forcing constitutive dimerization of the NTDs, has no major adverse effect on cell growth and only modestly impairs client activation[45]. This observation, plus the marginal impact of ATP binding in driving dimer closure, the typically quite weak ATP affinity, and the fact that the open and closed states are roughly isoenergetic, implies that the open-to-close transition is unlikely to be the ATP-driven mechanism for client remodeling by Hsp90.

The conformational changes directly linked to ATP-hydrolysis, especially at client-interacting residues, seem better suited for such a mechanism. Studies on HtpG with the model client $\Delta 131\Delta$ [57] as well as the very recently determined atomic structure of the human Hsp90:Cdc37:Cdk4 kinase complex[59], have begun to map critical determinants of client binding residues at the juncture of the Middle and C-terminal domains. As noted by Lavery et al, this coincides with the region of maximal asymmetry in TRAP1[27]. Our observation of a hydrolysis-driven conformational switch in which ATP hydrolysis directly promotes a rearrangement of the client binding region provides a mechanism for actively inducing conformational changes in the client. Equally important is that flipping of the entire TRAP1 population allows clients preferentially bound to either protomer, depending on their size, conformation or other characteristics, to be remodeled via rearrangement of their binding interface. Thus, the first hydrolysis would be used for client remodeling while the second one would be used to reset the ATP-dependent cycle of TRAP1. Notably, there is some evidence that such a sequential ATP hydrolysis mechanism may be shared among other GHKL ATPases. Yeast topoisomerase II, an enzyme which unlinks double-stranded DNA catenanes, hydrolyzes two ATP sequentially[19], and the first ATP hydrolysis appears to be used to facilitate DNA transport in decatenation[4]. Whether this asymmetric mechanism is conserved throughout all GHKL family members remains to be seen.

A critical feature of our model is the presence of functional asymmetry within the Hsp90 homodimer. Such asymmetry can either be intrinsic to Hsp90 or induced by interactions with other components. Indeed, emerging evidence suggests that functional complexes are preferentially asymmetric[12, 24, 29, 59]. For the eukaryotic cytosolic enzymes, this asymmetry can be provided by the numerous Hsp90-specific cochaperones or asymmetric post-translational modifications[37]. By contrast, TRAP1 and its bacterial homologs have no known cochaperones. The results and data presented here suggest that, in the case of the mitochondrial and bacterial chaperones, this necessary functional asymmetry may be an intrinsic property encoded by the structural asymmetry of the closed state.

1.5 Materials and methods

Cloning and protein purification

The constructs for Human and Zebrafish TRAP1 were the same as previously used [27]. Covalent heterodimeric constructs were made by fusing SpyCatcher and SpyTag [64] domain via an 8-a.a Gly-Ser (GGSGSGSG) linker at the C-terminus of TRAP1. The SpyCatcher domain was obtained from the pDEST14 plasmid obtained via AddGene. The construct used for heterodimeric zebrafish TRAP1 crystallography (+/R417A) has modified linker lengths appended to its C-terminus to account for the offset in starting amino acid residues between SpyCatcher and SpyTag. The SpyCatcher fusion has only a 2 a.a. (GS) linker and the SpyTag fusion has a 6 a.a. (GGSGSS) linker. Proteins were expressed in E. coli BL21(DE3)-RIL. Cells were grown in TB media at 37 °C to OD600 of ˜0.8 and then induced with 0.5 mM IPTG for 8–12 hr at 16 °C. Proteins were purified by Nickel-affinity chromatography, anion exchange (MonoQ 10/100 GL, GE, Pittsburgh, PA) and gel filtration (S200 16/60, GE). Heterodimeric constructs were expressed separately and then combined in roughly stoichiometric amounts after imidazole elution and incubated overnight at 4 °C while dialyzing into a low-salt buffer (10 mM Tris pH 8.0, 1 mM DTT). The heterodimers are separated via anion exchange with KCl gradient from 5 mM to 250 mM in 14 column volumes.

Heterodimeric peaks were pooled and then incubated with TEV protease overnight at 4 °C to cleave the N-terminal His-tag. Finally, proteins were further purified by gel filtration before they were snap frozen with liquid N_2.

Crystallization and data collection

Wild-type zTRAP1 protein at 5 mg/mL in 50 mM HEPES pH 7.5, 50 mM KCl and 1 mM TCEP was incubated with 10 mM ATP and 10 mM EDTA for 1 hr at RT to allow TRAP1 closure before setting 2 μL hanging drops by mixing 1:1 with crystallization condition consisting of 0.2 M Na/K tartrate, 19% (v/v) PEG3350 and 36 mM hexammine cobalt. Heterodimeric (+/R417A) zTRAP1 was incubated with 10 mM ADP-BeF/$MgCl_2$ for 1 hr at 30 °C to allow dimer closure. After incubation, samples were spun at 16,000xg for 10 min and transferred to new tubes. The crystals were grown in 0.19 M potassium acetate with varying PEG3350 (20–22%) and benzamidine hydrochloride (5–25 mM) as an additive. For each well condition, three protein concentrations: 0.5, 1, and 1.5 mg/mL were used to set 2 ml (1:1 protein to condition) hanging drops per concentration. All diffraction data were collected at beamline 8.3.1 at the Advanced Light Source in Berkeley, CA (at 1.116 Å wavelength and 91.4K).

Structure determination and refinement

Wild-type zTRAP1 datasets were indexed using iMosflm 7.2[5], and solved using molecular replacement (Phenix 1.10 - Phaser-MR) with PDB:4IPE and refined with phenix.refine[1] and manual refinement in Coot 0.8.3. Ramachandran statistics for the refined zTRAP1 1-day structure are 94.6% favored, 5% allowed, 0.3% outlier. Ramachandran statis- tics for the refined zTRAP1 3-day structure are 95.4% favored, 3.5% allowed, 1.1% outlier. Ramachandran statistics for the refined zTRAP1 53-day structure are 94.8% favored, 4.3% allowed, 0.9% outlier. Heterodimeric (+/R417A) zTRAP1 dataset was indexed using XDS[23] and initially solved by molecular replacement with PDB:4J0B using using Phaser (simple interface) via CCP4i2alpha interface[62]. Then a sequential search with the SpyCatcher-SpyTag complex (PDB:4MLS [30]) is performed while

keeping the previous solution fixed. Refinements of the heterodimeric zTRAP1 were done with Refmac5[38] using TLS groups and jelly-body restraints. Ramachandran statistics for the refined zTRAP1 +/R417A structure are 94% favored, 4.2% allowed, 1.7% outlier. Data and refinement statistics for all crystals are summarized in Table1.1.

FRET sample preparation and experiments

Two cysteines were introduced to the cysteine-free heterodimeric hTRAP1 constructs: one at the NTD at Glu140 (E140C) and another on the MD at Lys413 (K413C). Analogous constructs for the zebrafish TRAP1 was created by introducing point mutants G151C and K428C. Purified proteins were labeled with an equal mixture of Alexa Fluor 555 and Alexa Fluor 647 maleimide (ThermoFisher, Waltham, MA) at 2X molar excess to cysteines and incubated overnight at 4 °C. Unreacted dyes were then quenched with addition of 5 mM β-MeOH and removed using HiTrap desalting column (2x5 mL). For FRET experiments, 0.5 mM of labeled heterodimers were used. Measurements were obtained using a Horiba Jobin Yvon FluoroMax four spectrofluorometer equipped with a chilling/heating water bath. Samples were excited at 532 nm and emission wavelengths were collected at 567 nm and 668 nm for donor and acceptor fluorescence, respectively. Relative FRET efficiencies are calculated by taking the ratio of acceptor to donor fluorescence intensity. The change in FRET is the change of this ratio relative to timepoint 0.

SAXS experiments and data processing

Protein samples were buffer exchanged via size-exclusion chromatography using S200 10/300 GL (GE Healthcare Life Sciences) prior to the experiment. 6 mg/mL of heterodimeric hTRAP1 (+/R402A) was incubated at 30 °C for 3 hr with 1 mM ADP-BeF in reaction buffer (20 mM potassium phosphate pH 7.0, 50 mM KCl, 2 mM $MgCl_2$, 1 mM DTT). After incubation, samples were spun down at 16,000xg for 10 min and transferred to a new tube. Each experiment was collected with a total of 90-min exposure (15 s x 360 frames) using an in-house (Anton Paar SAXSESS mc2, Graz, Austria) SAXS instrument. Fitting of scattering intensity was done using a custom-written

software written in Python2.7 and Fortran (a copy is archived at https://github.com/elifesciences-publications/UCSFsaxs). The software applies smearing correction accounting for slit-collimated geometry of the X-ray beam, and it uses a Bayesian algorithm to choose an optimal D_{max} and smoothness of the P(r)[18]. The software also estimates protein molecular mass from an invariant, Q_r [46].

DEER sample preparation and measurements

Cysteine-free variants of heterodimeric hTrap1 were used for site-directed spin-labeling with maleimide spin-labels (4-maleimido-TEMPO, Sigma-Aldrich, Saint Louis, MO) after introduction of cysteines at positions K439 and D684. Prior to labeling, proteins were incubated with 5 mM DTT for 15 min at 4 °C, and DTT was then removed using a HiTrap desalting column (2x5 mL) equilibrated with N_2-purged labeling buffer (20 mM HEPES pH 7.5, 100 mM KCl). Spin labels were incorporated by immediate addition of threefold molar excess spin-label and incubated at 4 ° overnight. Unreacted probes were removed using HiTrap Desalting (2x5 mL) columns equilibrated with DEER reaction buffer (20 mM potassium phosphate pH 7.0, 50 mM KCl, 2 mM $MgCl_2$). Separation of free labels and extent of labeling was assessed by continuous wave (CW) EPR using a Bruker EMX EPR spectrometer (9.83 GHz). Labeled proteins were then buffer exchanged via a 30 kDa MWCO concentrator into the same buffer made in D_2O. Spin-labeled hTrap1 (˜140 mM dimer) was incubated with 1mMADP + 2mM BeF mix(2mM $BeCl_2$ + 10 mM KF) in presence of 2mM $MgCl_2$ for 1 hr at 30 °. Glycerol-d8 (Sigma-Aldrich) was then added to a final ˜30% (v/v) before snap freezing 10 ml samples in 1.1 mm ID quartz capillary tubes in liquid N_2. Four-pulse DEER data collection and analysis was done as previously described[27]. Data analysis was done with DeerAnalysis 2013 (http://www.epr.ethz.ch/software.html) in MATLAB to determine distance distributions as previously described[27].

Production of phoshate-binding protein and labeling for phosphate release assay

Phosphate release was assayed using phosphate-binding protein (PBP) labeled with MDCC (abcam, ab145370, Cambridge, MA) according to Brune *et al.* [6] with modifications in the protein purification and labeling. The PhoS gene was cloned from BL21 E. coli genomic DNA, and DeoD (E. coli purine nucleoside phosphorylase, ecPNPase) and DeoB (E. coli phosphodeoxyribomutase, ecPDRM) were synthesized using the BioXP3200 platform (SGI DNA, La Jolla, CA) and cloned into pet28a expression vectors with an N-terminal 6xHis tag. Ala197Cys point mutation in PhoS was introduced for site-specific labeling. All the purification and labeling used plastic containers instead of glass to minimize phosphate contamination, which reduces labeling efficiency. Proteins were purified via Ni^{2+}-affinity chromatography, and eluted with 400 mM Imidazole, and then run through HiTrap Desalting column equilibrated with 20 mM HEPES pH 7.5, 50 mM KCl. Proteins were then flash-frozen in liquid N_2. For labeling, PhoS.A197C (at ˜200 μM) was incubated with 1 μM PNPase, 0.5 μM PDRM, 50 μM $MnCl_2$, 50 μM α-D-glucose-1,6-bisphosphate and 0.5 mM 7-methylguanosine (Sigma-Aldrich) to mop-up contaminating phosphate. MDCC dissolved in DMSO was then added stepwise and gently mixed by inverting the tube, totaling up to 2X-molar excess of cysteines. The labeling reaction takes place at room temperature in the dark for 1 hr. Excess dyes were removed by loading the labeling reaction onto a HisTrap (5 mL) column and protein was eluted with a gradient of 20 mM to 500 mM imidazole. Labeled proteins were dialyzed into 20 mM HEPES pH 7.5, 50 mM KCl and concentrated up to ˜300 mM before freezing in aliquots.

For the phosphate release assay, a standard curve of free phosphate was prepared with 10 μM PBP-MDCC and varying concentrations of potassium phosphate. Fluorescence measurements were taken in the SpectraMax M5 platereader with SoftMax Pro software for data acquisition. Samples were excited at 375 nm and emission was recorded at 467 nm with ”Low” sensitivity setting. Only fluorescence counts below the detector linearity was used for analysis ($<$20000 RFU).

Steady-state ATPase assay and analysis

Steady-state ATPase activity was measured using enzyme-coupled NADH absorbance assay with 1 mM phosphoenolpyruvate (PEP), 0.18 mM NADH, 30 U/mL of both pyruvate kinase and lactate dehydrogenase. Kinetic absorbance measurements were carried out in Molecular Devices SpectraMax M5, at wavelengths 340 nm for NADH and 420 nm for background. Slopes were obtained from linear fits within linear regimes of each trace. Each reaction volume is 70 μL and a pathlength calibration is applied to convert absorbance to molar concentrations. For heterodimeric mixing experiment with TRAP1, wild-type and mutant proteins were mixed with different ratios while keeping total protein concentration constant. Each mixture was incubated at 30 °C for 1.5 hr to allow for dimer exchange. The final reaction has 2 μM dimer in ATPase reaction buffer (20 mM HEPES pH 7.5, 100 mM KCl, 5 mM $MgCl_2$). The total ATPase activity is fitted according to a binomial distribution of dimer species:

$$V_{\text{total}} = V_{\text{wildtype}} \cdot f_{\text{wildtype}}^2 + V_{\text{mutant}} \cdot f_{\text{mutant}}^2 + V_{\text{heterodimer}} \cdot f_{\text{mutant}} \cdot f_{\text{wildtype}}$$

where V denotes ATPase activity, f denotes the corresponding fractional population of wild-type and mutant. Since protein concentration is constant in all experiments, $f_{\text{wildtype}} = 1 - f_{\text{mutant}}$. Heterodimeric protein activity is simply the average of V_{wildtype} and V_{mutant} if assuming independence between activities.

Single-turnover radioactive ATPase assay

For radioactive atpase assays, reactions are initiated with addition of trace amounts [$\gamma -^3$ 2P]ATP (Perkin Elmer, 10 mCi/mL EasyTide Lead, Waltham, MA) mixed with cold ATP totalling up to ˜300 μM. The final radioactivity per 30 mL reaction is 0.1 mCi/mL. The ratio of TRAP1 dimer to ATP concentration is kept at 0.5:1, with slight protein excess at concentrations well above the Km for ATP to ensure single- turnover condition. Time points were taken by chemically quenching 1.5 mL aliquots with an equal volume of 40 mM Tris pH 8.0, 100 mM EDTA, 2% SDS and 2.5

mg/mL proteinase K. Aliquots (1 ml) of quenched reactions were spotted at 1 cm from the bottom of a PEI Cellulose F TLC plate (Millipore, Billerica, MA), and 6% formic acid, 0.5 M LiCl was used as mobile phase. The radioactive phosphate migrates about ˜0.8 of plate length from the origin. Radioactive signal was quantified via exposing the plates to a storage phosphor screen (Amersham, Pittsburgh, PA) for ˜1 min, and plate images were scanned with Typhoon FLA 9000. Image quantification was done in ImageJ (Wayne Rasband, NIH. https://imagej.nih.gov/ij/).

Molecular dynamics simulation

MD simulations were performed in explicit solvent using the TIP3P water model[22] and the CHARMM22 force field with CMAP corrections for protein and ions[31, 32, 33]. The initial protein structure was modeling based on the crystal structure of zebrafish Trap1 (PDB ID: 4IYN)[27] and subsequently solvated in a cubic water box at 150mM NaCl salinity, neutralized with extra ions employing VMD[21]. All simulations were carried out with periodic boundary conditions in a constant particle number, temperature, and pressure ensemble (NPT). The initial energy minimization and equilibration were carried out on general purpose supercomputers using NAMD 2.10[43]. The system to be simulated was first subjected to 10000 steps of conjugate gradient minimization and equilibrated for 2 ns with harmonic restraints applied to all the heavy atoms of the protein. The simulation was then continued for 10 ns without restraints at a constant pressure of 1 bar using Nosé–Hoover Langevin piston barostat and at a constant temperature (310 K or 360 K) maintained using Langevin dynamics with a damping constant of 1.0 ps^{-1}. Multiple time stepping was employed with an integration time step of 2.0 fs, short-range forces being evaluated every time step and long-range electrostatics evaluated every three time steps. Cutoff for short-range nonbonded interactions was 10.0 Å; long-range electrostatics was calculated using the particle-mesh Ewald method[10]. All bonds involving hydrogen in the protein were constrained using RATTLE[3], while the geometries of water molecules were maintained using SETTLE[36]. The resulting equilibrated structure was employed as the initial state for production simulations, carried out on the special purpose supercomputer Anton[53, 52] for ˜1.1 μs, where constant temperature

(310 K or 360 K) and constant pressure (P = 1 bar) were maintained. Multiple time stepping was employed, with an integration time step of 2.0 fs. Short-range forces were evaluated every time step and long-range electrostatics every three time steps. Cutoff for the short-range nonbonded interactions was 9.5 Å; long-range electrostatics was calculated using the k-Gaussian Split Ewald method[51] with a 64 x 64 x 64 grid. All bonds involving hydrogen atoms were constrained using SHAKE[50].

1.6 Supplemental Figures

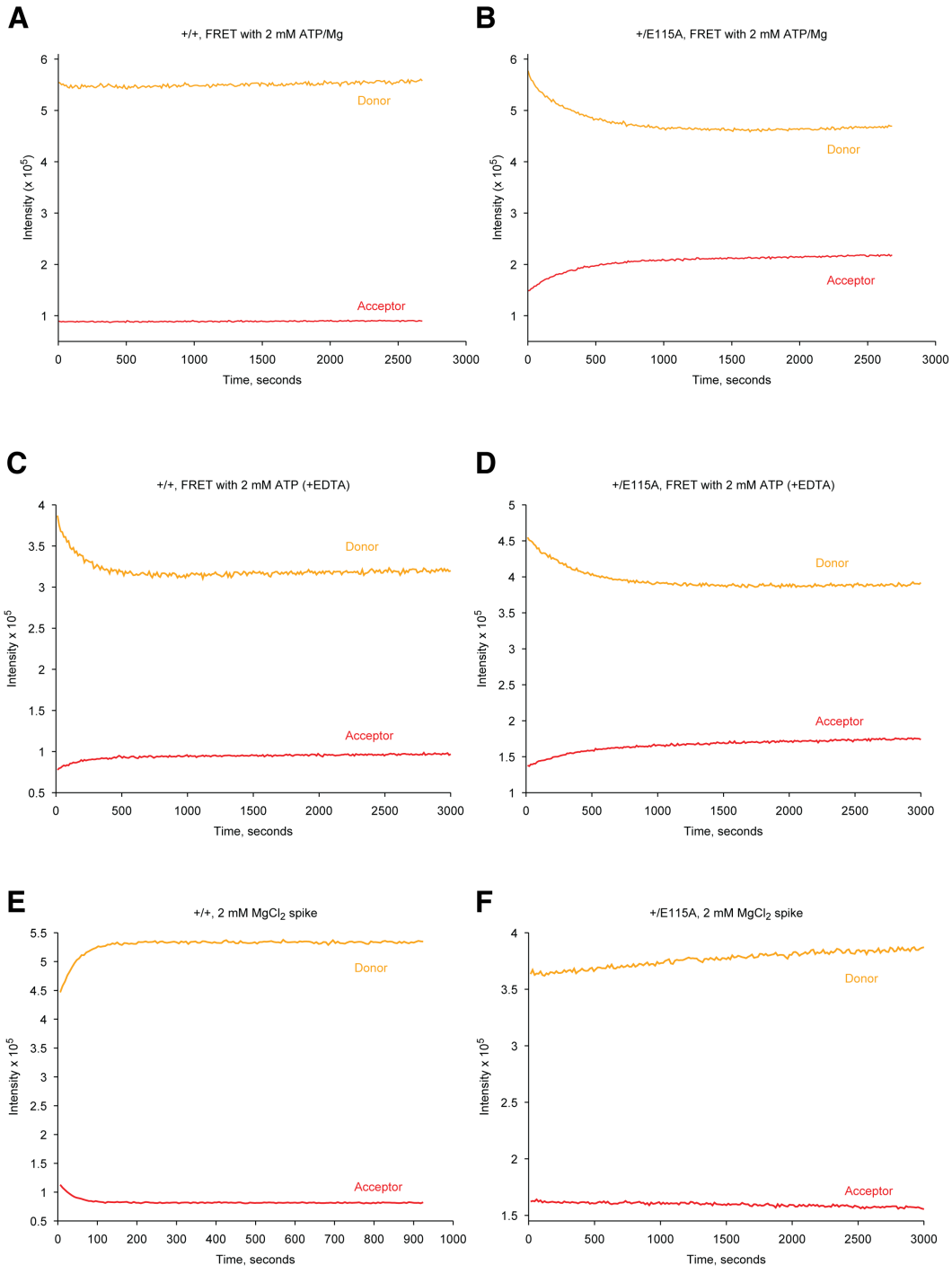

Figure S1.1: Raw fluorescence intensities of FRET data in Figure 1.1D-F. Donor intensities are colored orange and acceptor intensities are colored red. **A**–**B**) Raw fluorescence intensities of wild-

(**Figure S1.1**, *continued*) type (+/+, A) and hemi-hydrolyzing heterodimer (+/E115A, B) in presence of ATP/Mg added at t = 0 s from Figure 1.1D. (**C**–**D**) Raw fluorescence intensities of +/+ (**C**) and +/E115A (**D**) showing dimer closure after addition of ATP at t = 0 s in absence of $MgCl_2$ (with EDTA added) in Figure 1.1E. (**E**–**F**) Raw fluorescence intensities of +/+ (**E**) and +/E115A (**F**) showing dimer reopening after addition of 2 mM of MgCl2 at t = 0 s.

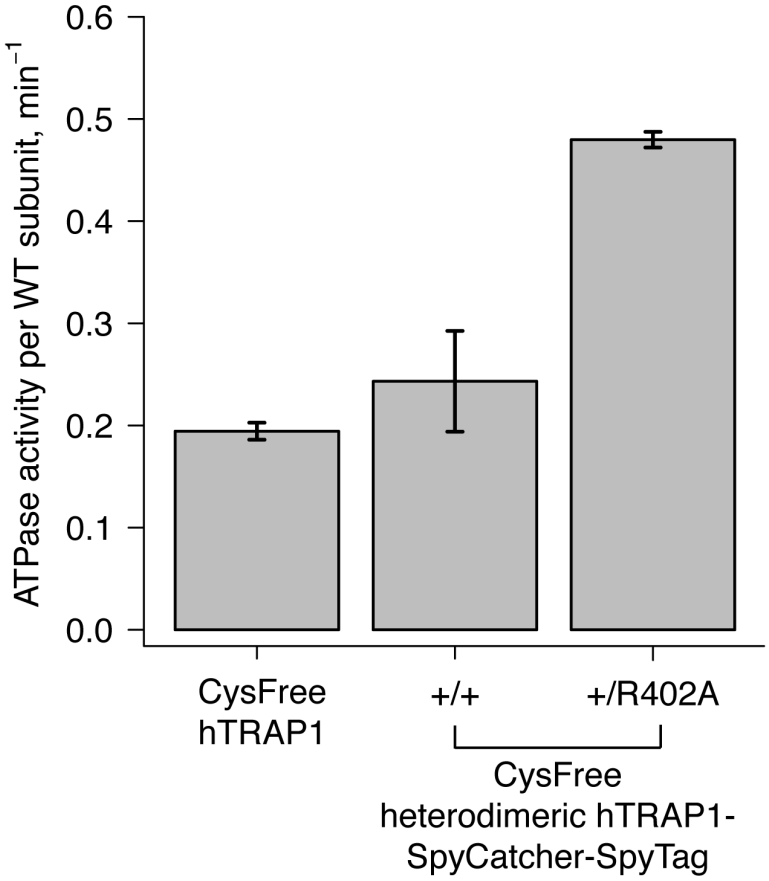

Figure S1.2: Steady-state ATPase assays of cysteine-free hTRAP1 and heterodimeric hTRAP1 (+/+ and + /R402A) at 30 °C. Each bar and error bar are one standard deviation and averaged from triplicate experiments. ATPase activities displayed are normalized per wild-type subunit.

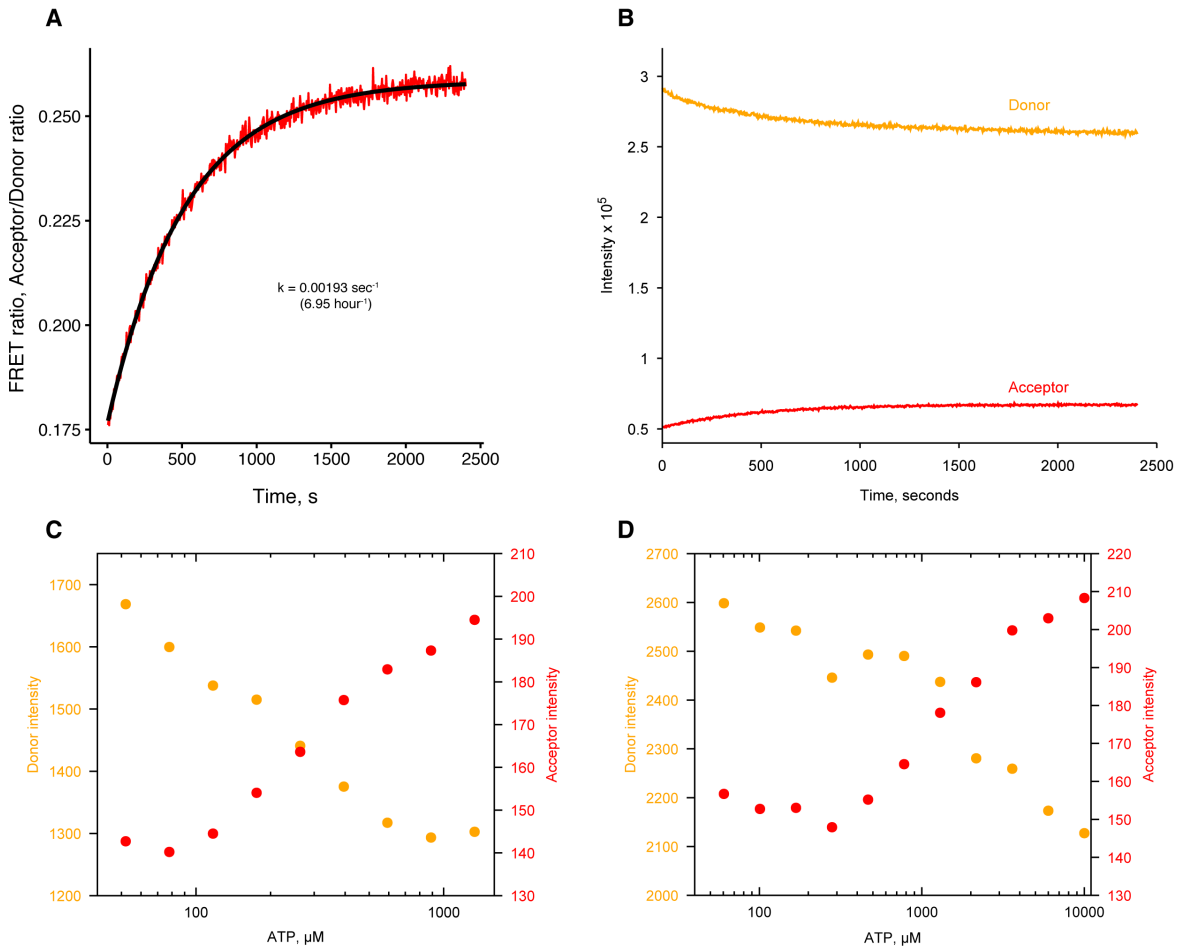

Figure S1.3: ATP-induced dimer closure in absence of Mg^{2+} by FRET in human and zebrafish TRAP1. (**A**) hTRAP1 dimer closure as seen by FRET after addition of 500 μM ATP at 30 °C. Closure rate is much faster than hydrolysis rate in absence of Mg^{2+}. Black line is the fit to an exponential function with the given rate constant. (**B**) Raw donor (orange) and acceptor (red) fluorescence intensities of FRET data in A. (**C**) Raw donor (orange) and acceptor (red) intensities of ATP titration to human TRAP1 from Figure 1.3A. (**D**) Raw donor (orange) and acceptor (red) intensities of ATP titration to zebrafish TRAP1.

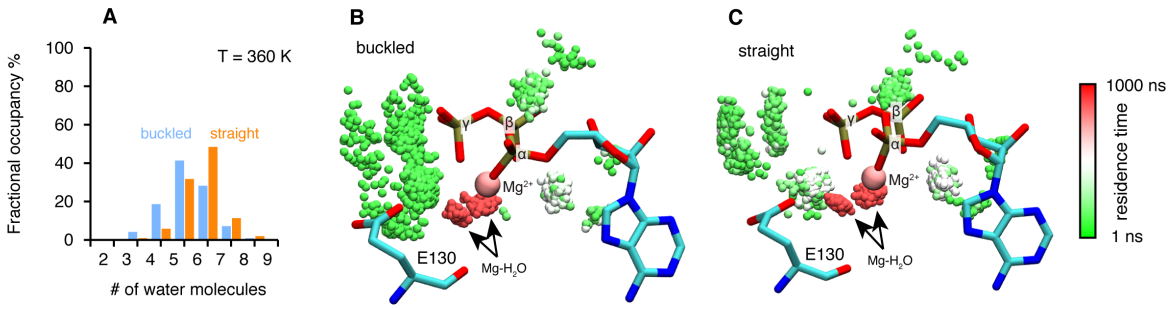

Figure S1.4: Microsecond all-atom molecular dynamics simulations of zTrap1 reveal asymmetric water dynamics near the ATP γ-phosphate at 360 K. (**A**) Fractional occupancy of water molecules near the ATP β- and γ-phosphate ($<$5 Å) within each 3 ns window in the buckled protomer A (blue) and the straight protomer B (orange). (**B**) and (**C**) Dwell time of each individual water molecule in ATP-binding pocket for buckled protomer and straight at T = 360 K. The figures were rendered by showing the water molecules (only oxygen for clarity) near the ATP β- and γ-phosphate ($<$5 Å) of all frames along the trajectory after aligning the system based on ATP. Black arrows point to magnesium-coordinated water molecules, Mg-H_2O. The water molecules were colored based on how long they stay in the vicinity of the ATP.

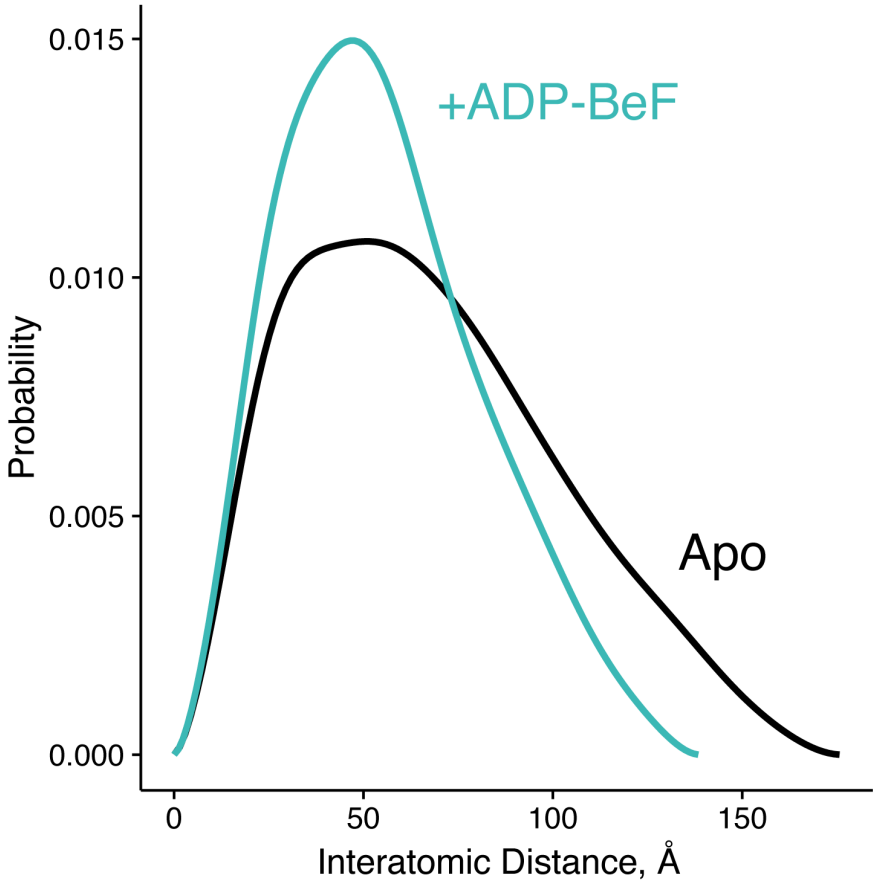

Figure S1.5: Interatomic distance distribution, P(r), from SAXS experiments of heterodimeric +/R402A human TRAP1. The heterodimer is fully capable of closing, shown as overall reduction in the width and maximum dimension of the P(r) distribution upon incubation with an ATP analog (ADP-BeF, teal). The black curve is the P(r) of the apo dimer.

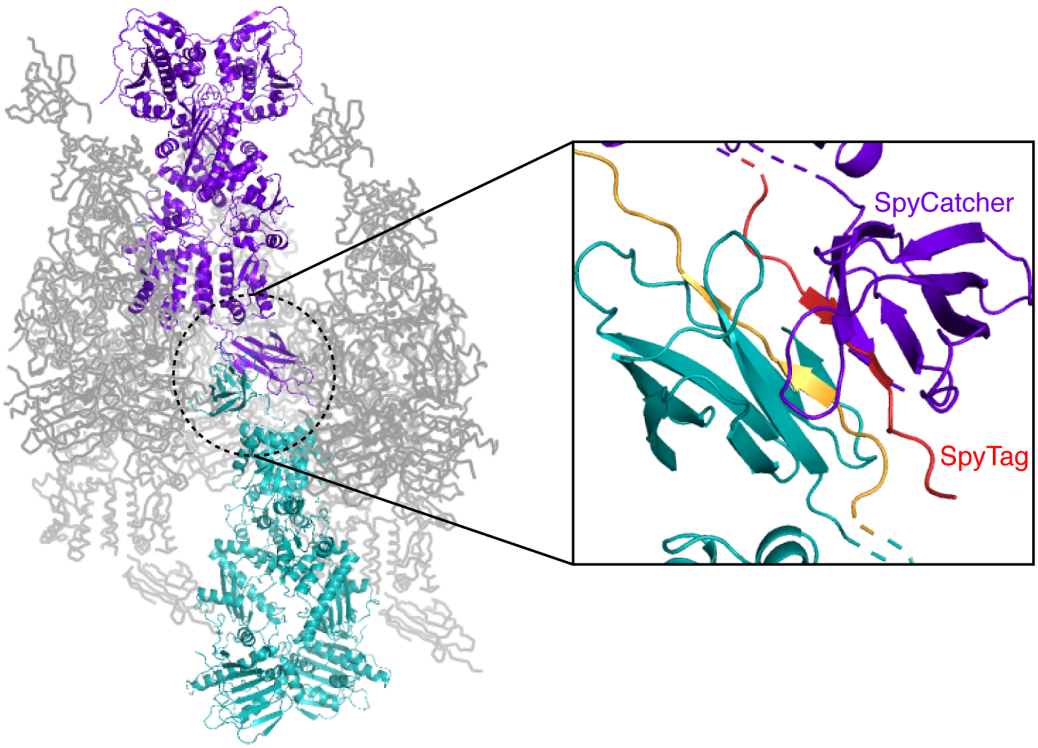

Figure S1.6: Crystal packing interactions for the heterodimeric (+/R417A) zTRAP1 fused to the SpyCatcher-Tag domains. A pair of symmetry mates is colored purple and teal whose SpyCatcher-Tag domains pack against each other (black inset, a close-up of the dotted circle). The SpyCatcher and SpyTag belonging to one dimer are colored purple and red, respectively. The corresponding SpyCatcher-SpyTag symmetry mate is colored teal and yellow, respectively.

	Heterodimeric zTRAP1 +/R417A	WT zTRAP1 (Day 1)	WT zTRAP1 (Day 3)	WT zTRAP1 (Day 53)
Data Collection				
Space group	C 1 2 1	C 1 2 1	C 1 2 1	C 1 2 1
Cell dimensions				
a,b,c (Å)	180.086, 95.711, 126.558	175.881, 96.9902, 124.961	178.49, 97.181, 125.904	178.491, 96.82, 125.78
α, β, γ (°)	90.0, 134.592, 90.0	90, 134.568, 90	90, 134.568, 90	90, 134.18, 90
Resolution (Å)	49.0 - 3.20	44.52 - 2.3	42.67 - 2.14	40.54 - 1.99
R_{sym} or R_{merge}	0.146	0.516	0.043	0.055
I / $\sigma(I)$	9.1 (1.0)	2.2 (0.29)	11 (0.76)	7.8 (0.29)
Completeness (%)	83.03	93.4	99.5	99.6
Redundancy	2.5	1.8	1.9	1.9
Refinement				
Resolution (Å)	49.0 - 3.20	39.67 - 3.5	39.89 - 2.5	39.97 - 2.2
No. of reflections	21134 (2095)	18821 (1856)	98531 (9720)	77679 (7714)
R_{work}/R_{free}	0.213/0.257	0.1977/0.2558	0.1804/0.2377	0.1885/0.2365
No. atoms				
Protein	10383	9592	9597	9570
Ligand/ion	66	62	66	62
Water	-	-	-	-
B-factors				
Protein	87.70	72.29	68.56	66.32
Ligand/ion	59.90	72.36	45.99	69.99
Water	-	62.38	52.91	55.34
r.m.s deviation				
Bond lengths (Å)	0.0122	0.003	0.008	0.007
Bond angles (°)	1.4721	0.604	1.01	0.96

Table 1.1: Crystallographic data collection and refinement statistics

*Each dataset was collected from a single crystal.
*Values in parentheses are for highest-resolution shell.

References

1. Adams, P. D. *et al.* PHENIX: a comprehensive Python-based system for macromolecular structure solution. *Acta crystallographica. Section D, Biological crystallography* **66,** 213–221 (Feb. 2010).

2. Ali, M. M. U., Roe, S. M., Vaughan, C. K., Meyer, P., Panaretou, B., Piper, P. W., Prodromou, C. & Pearl, L. H. Crystal structure of an Hsp90-nucleotide-p23/Sba1 closed chaperone complex. *Nature* **440,** 1013–1017 (Apr. 2006).

3. Andersen, H. C. Rattle: A "velocity" version of the shake algorithm for molecular dynamics calculations. *Journal of Computational Physics* **52,** 24–34 (Oct. 1983).

4. Baird, C. L., Gordon, M. S., Andrenyak, D. M., Marecek, J. F. & Lindsley, J. E. The ATPase reaction cycle of yeast DNA topoisomerase II. Slow rates of ATP resynthesis and P(i) release. *The Journal of biological chemistry* **276,** 27893–27898 (July 2001).

5. Battye, T. G. G., Kontogiannis, L., Johnson, O., Powell, H. R. & Leslie, A. G. W. iMOSFLM: a new graphical interface for diffraction-image processing with MOSFLM. *Acta crystallographica. Section D, Biological crystallography* **67,** 271–281 (Apr. 2011).

6. Brune, M., Hunter, J. L., Corrie, J. E. T. & Webb, M. R. Direct, Real-Time Measurement of Rapid Inorganic Phosphate Release Using a Novel Fluorescent Probe and Its Application to Actomyosin Subfragment 1 ATPase. *Biochemistry* **33,** 8262–8271 (May 2002).

7. Chen, B., Doucleff, M., Wemmer, D. E., De Carlo, S., Huang, H. H., Nogales, E., Hoover, T. R., Kondrashkina, E., Guo, L. & Nixon, B. T. ATP Ground- and Transition States of Bacterial Enhancer Binding AAA+ ATPases Support Complex Formation with Their Target Protein, σ54. *Structure (London, England : 1993)* **15,** 429–440 (Apr. 2007).

8. Cunningham, C. N., Krukenberg, K. A. & Agard, D. A. Intra- and Intermonomer Interactions Are Required to Synergistically Facilitate ATP Hydrolysis in Hsp90. *Journal of Biological Chemistry* **283,** 21170–21178 (July 2008).

9. Cunningham, C. N., Southworth, D. R., Krukenberg, K. A. & Agard, D. A. The conserved arginine 380 of Hsp90 is not a catalytic residue, but stabilizes the closed conformation required for ATP hydrolysis. *Protein science : a publication of the Protein Society* **21,** 1162–1171 (Aug. 2012).

10. Darden, T., York, D. & Pedersen, L. Particle mesh Ewald: An N·log(N) method for Ewald sums in large systems. *The Journal of Chemical Physics* **98,** 10089–10092 (June 1993).

11. Dollins, D. E., Warren, J. J., Immormino, R. M. & Gewirth, D. T. Structures of GRP94-nucleotide complexes reveal mechanistic differences between the hsp90 chaperones. *Molecular Cell* **28,** 41–56 (Oct. 2007).

12. Ebong, I.-o., Morgner, N., Zhou, M., Saraiva, M. A., Daturpalli, S., Jackson, S. E. & Robinson, C. V. Heterogeneity and dynamics in the assembly of the heat shock protein 90 chaperone complexes. *Proceedings of the National Academy of Sciences* **108,** 17939–17944 (Nov. 2011).

13. Eckl, J. M., Rutz, D. A., Haslbeck, V., Zierer, B. K., Reinstein, J. & Richter, K. Cdc37 (Cell Division Cycle 37) Restricts Hsp90 (Heat Shock Protein 90) Motility by Interaction with N-terminal and Middle Domain Binding Sites. *The Journal of biological chemistry* **288,** 16032–16042 (May 2013).

14. Elnatan, D., Betegon, M., Liu, Y., Ramelot, T., Kennedy, M. A. & Agard, D. A. Symmetry broken and rebroken during the ATP hydrolysis cycle of the mitochondrial Hsp90 TRAP1. *eLife* **6,** e25235 (July 2017).

15. Fisher, A. J., Smith, C. A., Thoden, J., Smith, R., Sutoh, K., Holden, H. M. & Rayment, I. X-ray Structures of the Myosin Motor Domain of Dictyostelium discoideum Complexed with MgADP.cntdot.BeFx and MgADP.cntdot.AlF4-. *Biochemistry* **34,** 8960–8972 (May 2002).

16. Frey, S., Leskovar, A., Reinstein, J. & Buchner, J. The ATPase cycle of the endoplasmic chaperone Grp94. *The Journal of biological chemistry* **282,** 35612–35620 (Dec. 2007).

17. Genest, O., Reidy, M., Street, T. O., Hoskins, J. R., Camberg, J. L., Agard, D. A., Masison, D. C. & Wickner, S. Uncovering a Region of Heat Shock Protein 90 Important for Client Binding in E. coli and Chaperone Function in Yeast. *Molecular Cell* **49,** 464–473 (Feb. 2013).

18. Hansen, S. Bayesian estimation of hyperparameters for indirect Fourier transformation in small-angle scattering. *Journal of Applied Crystallography* (2000).

19. Harkins, T. T., Lewis, T. J. & Lindsley, J. E. Pre-steady-state analysis of ATP hydrolysis by Saccharomyces cerevisiae DNA topoisomerase II. 2. Kinetic mechanism for the sequential hydrolysis of two ATP. *Biochemistry* **37,** 7299–7312 (May 1998).

20. Hessling, M., Richter, K. & Buchner, J. Dissection of the ATP-induced conformational cycle of the molecular chaperone Hsp90. *Nature Structural & Molecular Biology* **16,** 287–293 (Mar. 2009).

21. Humphrey, W., Dalke, A. & Schulten, K. VMD: Visual molecular dynamics. *Journal of molecular graphics* **14,** 33–38 (Feb. 1996).

22. Jorgensen, W. L., Chandrasekhar, J., Madura, J. D., Impey, R. W. & Klein, M. L. Comparison of simple potential functions for simulating liquid water. *The Journal of Chemical Physics* **79,** 926–935 (July 1983).

23. Kabsch, W. & IUCr. XDS. *Acta crystallographica. Section D, Biological crystallography* **66,** 125–132 (Feb. 2010).

24. Kirschke, E., Goswami, D., Southworth, D., Griffin, P. R. & Agard, D. A. Glucocorticoid Receptor Function Regulated by Coordinated Action of the Hsp90 and Hsp70 Chaperone Cycles. *Cell* **157,** 1685–1697 (June 2014).

25. Krukenberg, K. A., Böttcher, U. M. K., Southworth, D. R. & Agard, D. A. Grp94, the endoplasmic reticulum Hsp90, has a similar solution conformation to cytosolic Hsp90 in the absence of nucleotide. *Protein Science* **18,** 1815–1827 (Sept. 2009).

26. Krukenberg, K. A., Förster, F., Rice, L. M., Sali, A. & Agard, D. A. Multiple conformations of E. coli Hsp90 in solution: insights into the conformational dynamics of Hsp90. *Structure (London, England : 1993)* **16,** 755–765 (May 2008).

27. Lavery, L. A., Partridge, J. R., Ramelot, T. A., Elnatan, D., Kennedy, M. A. & Agard, D. A. Structural asymmetry in the closed state of mitochondrial Hsp90 (TRAP1) supports a two-step ATP hydrolysis mechanism. *Molecular Cell* **53,** 330–343 (Jan. 2014).

28. Leskovar, A., Wegele, H., Werbeck, N. D., Buchner, J. & Reinstein, J. The ATPase cycle of the mitochondrial Hsp90 analog Trap1. *The Journal of biological chemistry* **283,** 11677–11688 (Apr. 2008).

29. Li, J., Richter, K. & Buchner, J. Mixed Hsp90-cochaperone complexes are important for the progression of the reaction cycle. *Nature Structural & Molecular Biology* **18,** 61–66 (Jan. 2011).

30. Li, L., Fierer, J. O., Rapoport, T. A. & Howarth, M. Structural analysis and optimization of the covalent association between SpyCatcher and a peptide Tag. *Journal of Molecular Biology* **426,** 309–317 (Jan. 2014).

31. MacKerell, A. D. *et al.* All-atom empirical potential for molecular modeling and dynamics studies of proteins. *The journal of physical chemistry. B* **102,** 3586–3616 (Apr. 1998).

32. Mackerell, A. D. Empirical force fields for biological macromolecules: overview and issues. *Journal of computational chemistry* **25,** 1584–1604 (Oct. 2004).

33. Mackerell, A. D., Feig, M. & Brooks, C. L. Improved treatment of the protein backbone in empirical force fields. *Journal of the American Chemical Society* **126,** 698–699 (Jan. 2004).

34. McLaughlin, S. H., Smith, H. W. & Jackson, S. E. Stimulation of the weak ATPase activity of human hsp90 by a client protein. *Journal of Molecular Biology* **315,** 787–798 (Jan. 2002).

35. Mickler, M., Hessling, M., Ratzke, C., Buchner, J. & Hugel, T. The large conformational changes of Hsp90 are only weakly coupled to ATP hydrolysis. *Nature Structural & Molecular Biology* **16,** 281–286 (Mar. 2009).

36. Miyamoto, S. & Kollman, P. A. Settle: An analytical version of the SHAKE and RATTLE algorithm for rigid water models. *Journal of computational chemistry* **13,** 952–962 (Oct. 1992).

37. Mollapour, M. *et al.* Asymmetric Hsp90 N Domain SUMOylation Recruits Aha1 and ATP-Competitive Inhibitors. *Molecular Cell* **53,** 317–329 (Jan. 2014).

38. Murshudov, G. N., Vagin, A. A., Dodson, E. J. & IUCr. Refinement of Macromolecular Structures by the Maximum-Likelihood Method. *Acta crystallographica. Section D, Biological crystallography* **53,** 240–255 (May 1997).

39. Nathan, D. F. & Lindquist, S. Mutational analysis of Hsp90 function: interactions with a steroid receptor and a protein kinase. *Molecular and cellular biology* **15,** 3917–3925 (July 1995).

40. Panaretou, B., Prodromou, C., Roe, S. M., O'Brien, R., Ladbury, J. E., Piper, P. W. & Pearl, L. H. ATP binding and hydrolysis are essential to the function of the Hsp90 molecular chaperone in vivo. *The EMBO journal* **17,** 4829–4836 (Aug. 1998).

41. Pannier, M., Veit, S., Godt, A., Jeschke, G. & Spiess, H. W. Dead-time free measurement of dipole–dipole interactions between electron spins. *Journal of Magnetic Resonance* **213,** 316–325 (Dec. 2011).

42. Partridge, J. R., Lavery, L. A., Elnatan, D., Naber, N., Cooke, R. & Agard, D. A. A novel N-terminal extension in mitochondrial TRAP1 serves as a thermal regulator of chaperone activity. *eLife* **3** (2014).

43. Phillips, J. C., Braun, R., Wang, W., Gumbart, J., Tajkhorshid, E., Villa, E., Chipot, C., Skeel, R. D., Kalé, L. & Schulten, K. Scalable molecular dynamics with NAMD. *Journal of computational chemistry* **26,** 1781–1802 (Dec. 2005).

44. Prodromou, C., Panaretou, B., Chohan, S., Siligardi, G., O'Brien, R., Ladbury, J. E., Roe, S. M., Piper, P. W. & Pearl, L. H. The ATPase cycle of Hsp90 drives a molecular 'clamp' via

transient dimerization of the N-terminal domains. *The EMBO journal* **19,** 4383–4392 (Aug. 2000).

45. Pullen, L. & Bolon, D. N. Enforced N-domain proximity stimulates Hsp90 ATPase activity and is compatible with function in vivo. *Journal of Biological Chemistry* **286,** 11091–11098 (Apr. 2011).

46. Rambo, R. P. & Tainer, J. A. Accurate assessment of mass, models and resolution by small-angle scattering. *Nature* **496,** 477–481 (Apr. 2013).

47. Retzlaff, M., Hagn, F., Mitschke, L., Hessling, M., Gugel, F., Kessler, H., Richter, K. & Buchner, J. Asymmetric Activation of the Hsp90 Dimer by Its Cochaperone Aha1. *Molecular Cell* **37,** 344–354 (Feb. 2010).

48. Richter, K. Coordinated ATP Hydrolysis by the Hsp90 Dimer. *Journal of Biological Chemistry* **276,** 33689–33696 (July 2001).

49. Richter, K., Soroka, J., Skalniak, L., Leskovar, A., Hessling, M., Reinstein, J. & Buchner, J. Conserved conformational changes in the ATPase cycle of human Hsp90. *The Journal of biological chemistry* **283,** 17757–17765 (June 2008).

50. Ryckaert, J.-P., Ciccotti, G. & Berendsen, H. J. C. Numerical integration of the cartesian equations of motion of a system with constraints: molecular dynamics of n-alkanes. *Journal of Computational Physics* **23,** 327–341 (Mar. 1977).

51. Shan, Y., Klepeis, J. L., Eastwood, M. P., Dror, R. O. & Shaw, D. E. Gaussian split Ewald: A fast Ewald mesh method for molecular simulation. *The Journal of Chemical Physics* **122,** 54101 (Feb. 2005).

52. Shaw, D. E., Dror, R. O., Salmon, J. K. & Grossman, J. P. *Proceedings of the conference on high performance computing networking, storage and analysis* 2009.

53. Shaw, D. E. *et al.* Anton, a special-purpose machine for molecular dynamics simulation. *Communications of the ACM* **51,** 91–97 (July 2008).

54. Shiau, A. K., Harris, S. F., Southworth, D. R. & Agard, D. A. Structural Analysis of E. coli hsp90 reveals dramatic nucleotide-dependent conformational rearrangements. *Cell* **127,** 329–340 (Oct. 2006).

55. Southworth, D. R. & Agard, D. A. Client-loading conformation of the Hsp90 molecular chaperone revealed in the cryo-EM structure of the human Hsp90:Hop complex. *Molecular Cell* **42,** 771–781 (June 2011).

56. Southworth, D. R. & Agard, D. A. Species-Dependent Ensembles of Conserved Conformational States Define the Hsp90 Chaperone ATPase Cycle. *Molecular Cell* **32,** 631–640 (Dec. 2008).

57. Street, T. O., Lavery, L. A. & Agard, D. A. Substrate binding drives large-scale conformational changes in the Hsp90 molecular chaperone. *Molecular Cell* **42,** 96–105 (Apr. 2011).

58. Street, T. O., Lavery, L. A., Verba, K. A., Lee, C.-T., Mayer, M. P. & Agard, D. A. Cross-Monomer Substrate Contacts Reposition the Hsp90 N-Terminal Domain and Prime the Chaperone Activity. *Journal of Molecular Biology* **415,** 3–15 (Jan. 2012).

59. Verba, K. A., Wang, R. Y.-R., Arakawa, A., Liu, Y., Shirouzu, M., Yokoyama, S. & Agard, D. A. Atomic structure of Hsp90-Cdc37-Cdk4 reveals that Hsp90 traps and stabilizes an unfolded kinase. *Science (New York, N.Y.)* **352,** 1542–1547 (June 2016).

60. Whitesell, L. & Lindquist, S. L. HSP90 and the chaperoning of cancer. *Nature Reviews Cancer* **5,** 761–772 (Oct. 2005).

61. Wiech, H., Buchner, J., Zimmermann, R. & Jakob, U. Hsp90 chaperones protein folding in vitro. *Nature* **358,** 169–170 (July 1992).

62. Winn, M. D. *et al.* Overview of the CCP4 suite and current developments. *Acta crystallographica. Section D, Biological crystallography* **67,** 235–242 (Apr. 2011).

63. Wittinghofer, A. Signaling mechanistics: Aluminum fluoride for molecule of the year. *Current Biology* **7,** R682–R685 (Nov. 1997).

64. Zakeri, B., Fierer, J. O., Celik, E., Chittock, E. C., Schwarz-Linek, U., Moy, V. T. & Howarth, M. Peptide tag forming a rapid covalent bond to a protein, through engineering a bacterial adhesin. *Proceedings of the National Academy of Sciences* **109,** E690–7 (Mar. 2012).

65. Zhao, R. *et al.* Navigating the chaperone network: an integrative map of physical and genetic interactions mediated by the hsp90 chaperone. *Cell* **120,** 715–727 (Mar. 2005).

Chapter 2

Differential regulation of TRAP1 ATPase activity by magnesium and calcium

2.1 Preface

This chapter is the culmination of a few side projects of mine that various rotation students through the lab have in one way or another contributed to. Since this was a side project, it was mainly driven by curiosity, my obsession with measuring ATPase activities and motivated by stimulating discussions with people that were interested in the mitochondria. The idea originated when Laura Lavery was concerned that components from the TCA cycle (like the reagents used in a routine NADH-coupled ATPase assays) may have an effect in intrinsic TRAP1 ATPase activity. She had a rotation student, David Mavor, to address this question by comparing rates of dimer closure rate by FRET to the ATPase activity with matching conditions (with coupled-assay reagents in the FRET assay). Calcium was tried in both assays with no apparent effect. That was the end of the exploration for a while. As time goes on, I continued to improve the ATPase assays that we had in the lab for better sensitivity and easier setup. The main motivation for me was that I loved doing ATP titration when setting up an ATPase assay because when the assay is easy enough for multiple points, and the end result is more informative than a single point measurement done at saturating ATP concentrations. When Laura and I were first doing ATPase measurements this way, we first noticed a persistent "bump" at around 50 μM ATP, though it was hard to convince ourselves

because the large error bars made it difficult to interpret. At the time, James Partridge and I were doing heterodimeric experiments mixing different point mutants that affect ATPase rates of TRAP1 or HtpG. There we saw an increased ATPase activity (up to 8 to 10-fold than wild-type) when wild-type protein is mixed with mutants that doesn't bind ATP. From this observation, Timothy Street and I formed a model that perhaps dimers that only bind 1 ATP can close faster, and thus having a higher ATPase rate. This observation lead to a series of rotation projects investigating the nature of this half-occupied dimer and how it can close faster. From Joe Lobel's rotation, we know this requires N-terminal Domain (NTD) of TRAP1 to be rotated as seen in the closed dimer state. Miguel Betegon measured the NTD:MD rotation rate by FRET and saw it matches exactly with the closure rate measured between the NTD and MD. Finally, Aditya Anand observed that this half-occupied closed dimer is not very stable (reopens with addition of excess ADP in a matter of tens of minutes), and that calcium can actually trigger dimer re-opening faster than magnesium. This rejuvenated my interest in calcium effect, since at the time, there I was reading a lot of literature on the physiological roles of calcium in the mitochondria.

When I finally had a real-time kinetic ATPase assays that don't depend on divalent cations to detect ATPase activity (the NADH-coupled enzymes need magnesium as a co-factor), I started measuring ATPase activities of TRAP1 and other Hsp90 in presence of calcium. There was the beginning of a foundation this project: I saw a clear and reproducible effect in how TRAP1 behaves in presence of calcium versus magnesium. This was the time that Laura Lavery was graduating, and she wanted to make sure that both Miguel and I know how to grow crystals. We started with her zebrafish TRAP1 crystals and learned to grow and loop crystals from those samples. Eventually, I began a screen to look for conditions that would crystallize zebrafish TRAP1 with AMPPNP in presence of calcium to figure out where it binds. This chapter contains my efforts in trying to figure out the molecular details of calcium binding and how it imparts the observed effects in TRAP1 ATPase activity. This work is not published (yet), and we plan to further refine and publish this manuscript.

2.2 Introduction

Most of enzymatic studies of ATPases typically include magnesium as the physiological co-factor. Since calcium is typically kept at very low concentrations in the cytoplasm, this is a reasonable choice for most enzymes, especially if they reside in the cytoplasm where calcium is kept at low nanomolar concentrations at resting state. However, sub-cellular organelles have vastly different environment due to their molecular composition. It is now well appreciated that mitochondria serve as a calcium reservoir for the cell. Calcium-phosphate granules form inside the mitochondrial matrix, that if it were dissolved, would reach molar concentrations[22]. It is well appreciated that mitochondrial enzymes are regulated by calcium ions[3]. In particular, a few mitochondrial dehydrogenases involved in ATP production are stimulated by calcium ions, suggesting a direct link to cellular energetics. Although calcium interactions and the resulting modulation on these enzymes are clear, many of the molecular mechanisms for these effects have not been elucidated, in part due to the lack of a clear binding site and the complexities of the model systems under study. Moreover, given the prevalence of calcium in the mitochondrial matrix, it is likely that calcium ions play important roles in regulating other proteins in the mitochondria. In this study, we look at how a mitochondrial homolog of the molecular chaperone Hsp90 (TRAP1) may be regulated by calcium binding.

The Hsp90 protein family is highly conserved and have adapted to vastly different sub-cellular environments within organelles (endoplasmic reticulum (ER), mitochondria, and chloroplast in plants). Hsp90 is a homodimer with each protomer composed of 3 globular domains: an ATP-binding N-terminal Domain (NTD), a middle domain (MD), and C-terminal dimerizing domain (CTD). Various adaptations on Hsp90 homologs and isoforms come by way insertions and/or deletions outside of the conserved globular domains that confer new features (e.g. interactions with co-chaperones, sub-cellular localizations, etc). ATPase activity of Hsp90 is absolutely essential for its function in eukaryotic cells. The majority of knowledge for *in-vivo* Hsp90 function and mechanism have been derived from the cytosolic isoform because of its importance in disease and

evolution[20]. From earlier studies, it is clear that despite being structurally conserved, Hsp90 homologs differ in their ATPase kinetics [11, 5, 15]. ATP hydrolysis occurs in Hsp90 within the closed state where the NTDs are dimerized, forming intra- and inter-protomer interactions that support the catalytically active state[2]. Differences in the ATPase activities between Hsp90 homologs likely reflect the distinct conformational equilibrium between the open and closed state for each species[17]. For TRAP1, this open-closed equilibrium is subject to thermal regulation imparted by an N-terminal extension[14]. Another unique feature of TRAP1 is that ATP alone, without any divalent cation co-factor, is sufficient to stabilize the closed state[14, 4]. The mechanism of this phenomenon is not known. Perhaps this is yet another mitochondria-specific adaptation given some free ATP (uncomplexed to Mg^{2+}) existing in the mitochondrial matrix[6]. The concentrations of divalent cations and nucleotide is heterogeneous and vary depending on the tissue or cell-type under study. To get a better understanding how divalent cations may regulate TRAP1, experimental systems with purified protein can bypass the complexity of cell-based models. Useful insights can be obtained from basic biophysical properties and provide a starting molecular model that may be important in the cellular context. To this end, we investigate how ATPase activity of TRAP1 is regulated by two divalent cations: magnesium or calcium. We find that unlike other Hsp90 homologs, TRAP1 ATPase has distinct activity profiles due to preferences for magnesium or calcium, and that this preference is determined by the concentration of free ATP. By crystallography, the binding site for calcium is revealed to be within the NTD complexed with AMPPNP. These observations lead to a model of how ATP-site occupancy within TRAP1 imparts preference for magnesium and calcium.

2.3 Results

TRAP1 has unique enzyme kinetics depending on magnesium or calcium

The physiological divalent metal cofactor for most ATPases are magnesium. However, given the role of mitochondria as a calcium reservoir for the cell, we decided to test whether it has any

effect in ATP hydrolysis by TRAP1. ATP hydrolysis by Hsp90 happens in the closed state when the NTDs are dimerized. This closed state can be stabilized by using a non-hydrolysable ATP analog, or in the case of TRAP1, simply omitting magnesium in the reaction allows the build-up of this closed state because ATP hydrolysis rate becomes much slower than the kinetics of dimer closure [14, 4]. We have previously taken advantage of this phenomenon to decouple dimer closure event from ATP hydrolysis, which can be initiated by addition of Mg^{2+} into the reaction. The closed dimer reopens when ATP hydrolysis resumes, and this can be monitored by a FRET assay (Figure 2.1A). Our initial efforts in looking at the effect of calcium did not show significant effects on the basal magnesium-supported steady-state ATPase activity of hTRAP1 (data not shown). Since the steady-state assay only reads out the slow step of dimer closure, we decided to test whether calcium can trigger dimer reopening starting from the closed state with ATP in the FRET assay. As previously observed, addition of magnesium to the reaction causes loss of FRET over time due to hydrolysis-triggered dimer re-opening. To our surprise, the addition of calcium can also cause dimer opening (Figure 2.1B), and with faster kinetics than magnesium. This suggests that calcium alone can support ATP hydrolysis by TRAP1.

To see whether calcium alone can support ATP hydrolysis by hTRAP1, ATPase activity of TRAP1 was measured in buffers with either excess magnesium or calcium as the sole divalent cation. As previously observed[11], the ATPase activity in presence of magnesium reaches a plateau with as little as ~50 μM ATP. By contrast, ATPase activity in presence of calcium follows the Hill-equation with n=1.4 and an ATPase rate that is 1.6-fold faster than in magnesium at saturating ATP concentration (Figure 2.1C, see Table 2.1 for fitted parameters). While fitting the data, we noted that the Michaelis-Menten equation is a poor fit to the magnesium ATPase activity. This behavior appears to be conserved in zebrafish TRAP1 (zTRAP1) (Figure S2.1). The "bump" on the curve between 0 to ~200 μM ATP can be explained by considering a model that accommodates a population of TRAP1 dimer bound to only one ATP, which has a higher ATPase activity than the two ATP-bound dimer. To test this idea, ATPase activity of heterodimeric hTRAP1 with only one ATP binding site per dimer (formed by equilibrating a mixture of wild-type protein with 15-fold molar

excess of the D158N point mutant) was measured as a function of ATP concentration. Indeed, in the presence of magnesium, the ATPase activity curve of the heterodimer no longer has the "bump" and follows a standard single-site Michaelis-Menten kinetics (Figure 2.1D, blue line). Moreover, the apparent affinity ($K_{0.5}$, defined as the concentration at half-max of activity) to ATP measured in this heterodimer (Table 2.3) close to the one estimated by the wild-type experiment (Table 1) (58 μM vs 73 μM). To further examine whether this discrimination of magnesium versus calcium is a unique feature of TRAP1, ATPase activities of a few Hsp90 homologs were also measured. Beyond the general trend that ATPase activity is lower when calcium is used, none of the tested homologs exhibited the distinct ATP concentration-dependent activity as seen in TRAP1 (Figure S2.2).

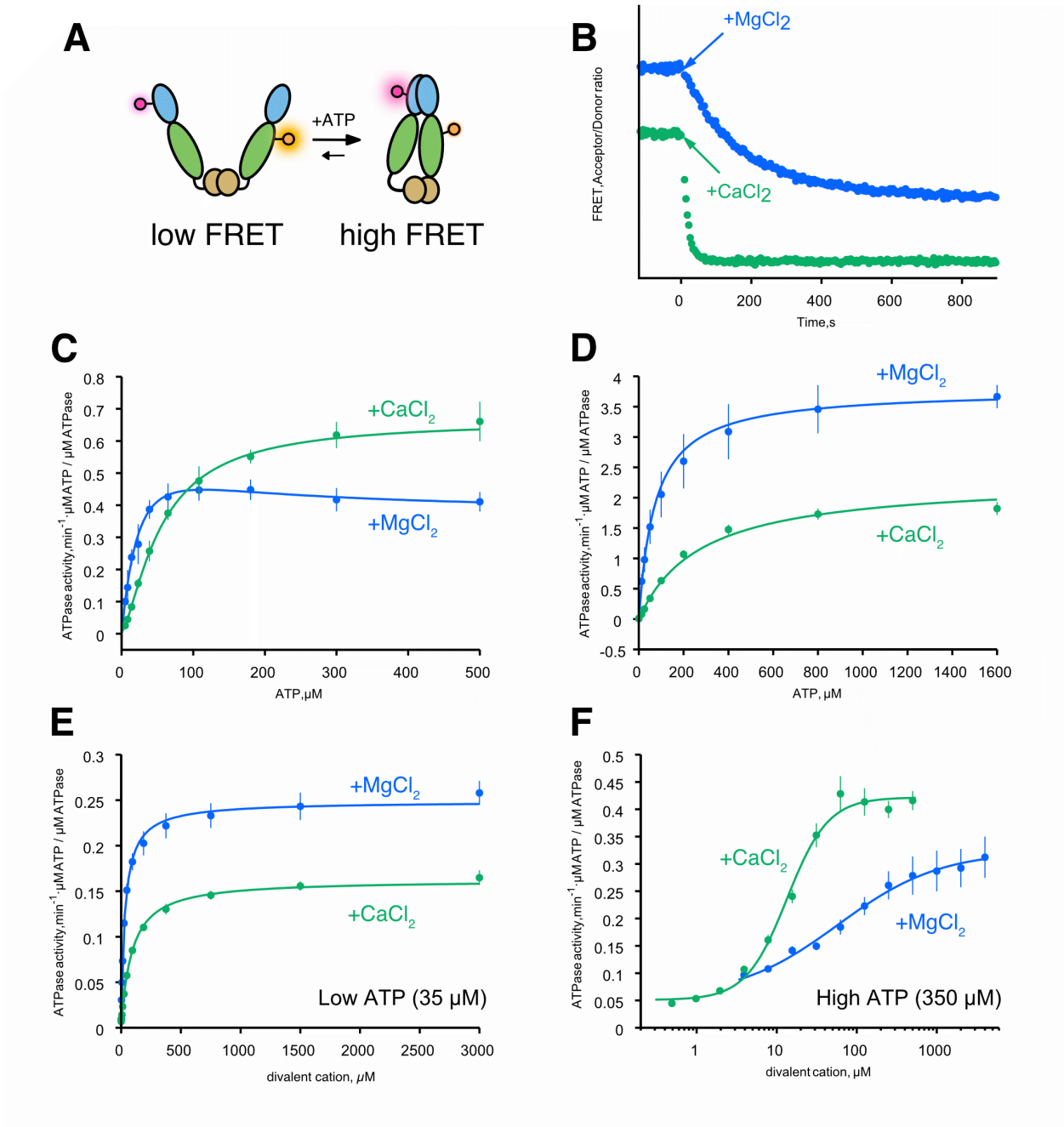

Figure 2.1: Calcium supports ATP hydrolysis by TRAP1. (**A**) Cartoon diagram of the FRET assay with TRAP1 to monitor open (low FRET) and closed state (high FRET). Dye molecules (glowing circles) are covalently attached at the middle domain (green ellipse) and the NTD (blue ellipse). (**B**) FRET re-opening assay starting from the closed state (high FRET). Reaction was initiated by addition of either $MgCl_2$ (blue) or $CaCl_2$ (green) at t=0. Time-dependent decrease of FRET signal indicate dimer opening. FRET is quantified as the ratio of Acceptor/Donor intensity. The kinetic trace has been vertically offset for clarity. (**C**) ATPase activity of hTRAP1 in presence of excess $MgCl_2$(blue) or $CaCl_2$(green) as a function of ATP concentration. (**D**) ATPase activity of wild-type:D158N heterodimeric mixture in presence of $MgCl_2$ or $CaCl_2$ as a function of ATP con-

(**Figure 2.1**, *continued*) centration. (**E**) ATPase activity of hTRAP1 at low ATP concentration (35 μM) as a function of divalent cation concentrations ($MgCl_2$ in blue; $CaCl_2$ in green). (**F**) ATPase activity of hTRAP1 at high ATP concentration (350 μM) as a function of divalent cation concentrations ($MgCl_2$ in blue; $CaCl_2$ in green).

ATP-site occupancy biases preference for magnesium versus calcium in TRAP1 ATPase activity

Given the observed ATP-concentration and divalent cation dependence of TRAP1 ATPase activity, we next examine how magnesium and calcium affect TRAP1 ATPase activity under sub-saturating (35 μM ATP in hTRAP1, or 50 μM ATP in zTRAP1) or saturating ATP concentrations (350 μM ATP). If there are indeed two populations of TRAP1 dimer that depends on ATP-concentration (bound to one or two ATP per dimer), then using a low or high ATP concentration should enrich for these populations, respectively. Accordingly, the apparent affinity ($K_{0.5}$) and occupancy (n) of the divalent cations can be approximated by fitting the Hill-equation to initial rates from titrations at fixed ATP concentrations. At low ATP concentrations, TRAP1 seems to prefer magnesium to calcium, showing tighter apparent affinity by about 1.7-fold in zTRAP1 (Mg, 39 μM vs Ca, 66 μM) and 2.8-fold in hTRAP1 (Mg, 33 μM vs. Ca, 92 μM), and also ˜1.5-fold higher activity in both species (see Table 2.2). Another trend observed from the fitting is that at low ATP concentrations, the Hill-coefficient tend to stay near one for both magnesium and calcium, suggesting that the cations are binding to the population of TRAP1 dimer with one ATP-bound. If magnesium is the preferred cation by the one-ATP-bound dimer, then the wt:D158N heterodimeric mixture should show both tighter apparent affinity to ATP and higher activity in magnesium than calcium. Indeed, this is just what was observed when ATPase activity of the heterodimer is compared between magnesium and calcium (Figure 2.1D, Table 2.3).

At high ATP concentrations, calcium is the preferred divalent cation with a tighter K0.5 by ˜7-fold in zTRAP1 (Mg, 235 μM vs Ca, 35 μM — see Table 2.2), and ˜4.5-fold for hTRAP1 (Mg, 59 μM vs Ca, 13 μM). The observed differences in apparent affinities between species most

likely reflect intrinsic properties of each protein. The turnover rates at high ATP concentration only show a subtle increase, with calcium supporting a ˜1.1-fold faster rate in both human and zebrafish. At high ATP concentrations, n also remains close to one for only magnesium while n=1.7 for calcium. From crystal structures of the closed state of TRAP1, the number of magnesium binding site is unambiguous: there are two per dimer on each NTD, coordinated between the β- and γ-phosphates of ATP. Therefore, the Hill-coefficient close to 1 at high ATP concentration likely reflects the sequential (non-cooperative) nature of ATP hydrolysis with magnesium[4]. To understand how calcium imparts an apparent cooperativity in TRAP1 ATPase activity, which has never been observed in other Hsp90 homologs, a clear binding site for calcium must be identified.

Calcium binds to the N-terminal Domain (NTD) of TRAP1

Since TRAP1 does not contain any apparent calcium-binding motifs, we sought to determine where calcium binds by crystallography. A novel screen set with zTRAP1 incubated with 2 mM AMPPNP/Ca yielded crystals in 0.2 M Na/K tartrate and 17% PEG-3350. And as previously observed[10], addition of hexammine cobalt improves diffraction quality of the crystals. The structure was solved using molecular replacement of previously determined closed-state of TRAP1, and reveals a virtually identical asymmetric closed state[10] (Figure 2.2A). Examining the nucleotide binding pocket, the electron density of the AMPPNP molecule lack densities where magnesium was previously observed (coordinated between the β- and γ-phosphates). This was unexpected given that for other ATPases (Hsp70/DnaK/actin family), calcium had been found to occupy the same site as magnesium [18, 1], between the β and γ phosphates. To localize potential calcium sites, we exploited anomalous X-ray scattering of calcium (Figure S2.3) and collected two datasets: one at 7450 eV (1.664 Å) and 11111 eV (1.116 Å). Although the anomalous difference is considerably weaker than what is required for experimental phasing, significant peaks can be estimated reliably for a well-determined structure using ANODE[19]. Using phases from the solved structure without the contribution of calcium atoms, the resulting anomalous density map reveals two strong peaks within the nucleotide pocket, one for each NTD located just above the α-phosphate (Figure 2.2A,

black inset). The density is coordinated by six oxygen atoms in an octahedral arrangement (4 carbonyl oxygens of sidechain amide groups near the "lid" of the NTD, one is from a hydroxyl group of a Tyrosine, and one oxygen from the α-phosphate) (Figure 2.2B). Despite the expectation of TRAP1 having a relatively weak affinity to calcium, a slightly higher B-factor (˜50 vs. the AMPPNP average ˜40 or ˜24 for the coordinating carbonyl oxygens) and longer bond lengths ($>$2.5 Å) between CA-O are seldom observed for a calcium binding site, making it difficult to unambiguously assign. To lend credence to these strong anomalous peaks, a negative control of identical crystals lacking calcium was needed. Luckily, we came across zTRAP1 crystals with identical conditions while performing another study [4]. The only differences with this crystal was that there were no calcium (excess EDTA was present) and the dimer was closed with ATP instead of AMPPNP. Using this as a negative control, the same anomalous X-ray dataset was collected and the anomalous density was generated after solving the structure by molecular replacement. From this dataset, no significant anomalous peaks were detected near the α-phosphate, indicating that in the original dataset, the unexplained strong electron density is indeed from a calcium atom.

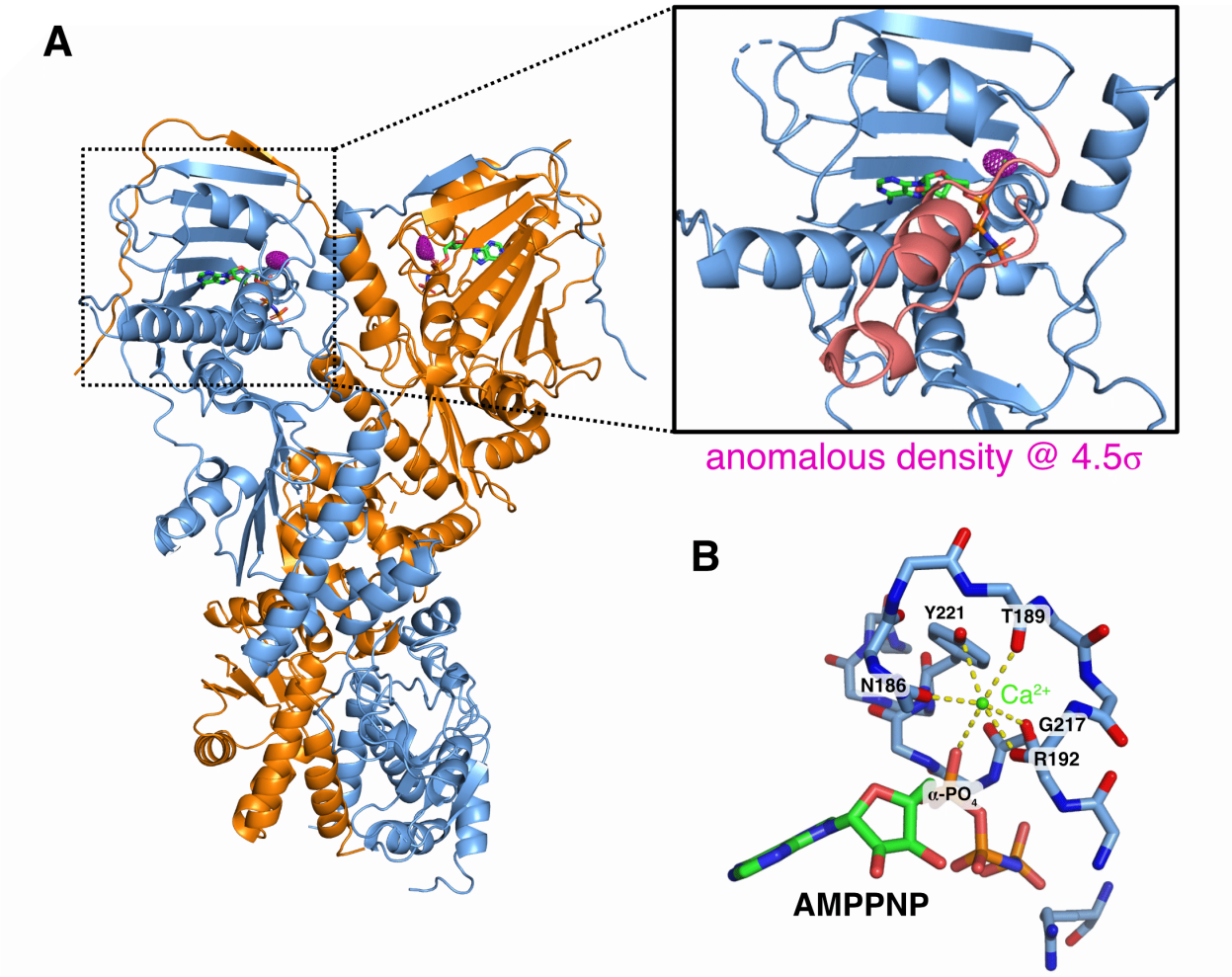

Figure 2.2: Calcium binds to the N-terminal domain of TRAP1. (**A**) Full-length structure of zTRAP1 bound to AMPPNP and Ca^{2+}. Each protomer/chain is colored blue and orange in a cartoon representation. The ATP-"lid" region of the NTD is colored in pink (black rectangular inset). The anomalous electron density map (displayed at 4.5σ contour level) for calcium is shown in purple mesh. (**B**) Coordination of calcium (green sphere) by residues in the ATP-"lid" and the α-phosphate of the AMPPNP. Yellow dashed lines depict contacts from oxygens to calcium atom. All of the oxygens were from backbone carbonyl of labeled residues with the exception of one hydroxyl oxygen from Tyr221.

2.4 Discussion

Most of enzymatic studies using Hsp90 have used magnesium as a co-factor. In this study, we have followed up an initial observation that calcium alone is sufficient to support TRAP1 ATPase activity. This calcium-supported activity appears to be unique to TRAP1 in that at saturating ATP concentrations, using calcium results in a modestly higher ATPase activity in contrast to other Hsp90 homologs, where the use of calcium generally results in a lower ATPase activity. Direct visualization of the calcium binding-site provides a molecular basis for the apparently cooperative ATPase behavior that is conferred by calcium binding(Figure 2.3). From the ATPase measurements at low ATP concentration, TRAP1 hydrolyzes ATP more efficiently with magnesium than with calcium. This can be explained with a model where calcium does not bind to the apo NTD: the coordinating oxygens located within the ATP-lid are not arranged in a cluster to chelate the calcium and the α-phosphate oxygen in ATP is needed to form the octahedral metal coordination. This way, the formation of calcium binding sites happen in a cooperative manner. Each NTD must be bound to ATP in order to stabilize the closed lid conformation via NTD dimerization. Once formed, fluctuations of the ATP lid create an opening for calcium entry just above the α-phosphate location. This model may explain the apparent faster re-opening kinetics when calcium is added to trigger dimer hydrolysis-dependent reopening when compared to magnesium. It is much more difficult for magnesium to diffuse into its binding site, between the β- and γ-phoshate of ATP, within the closed-lid state because this cavity has significant steric roadblocks. Therefore, the easier path for magnesium binding is when complexed with ATP into the apo NTD where the lid is open. Perhaps this is why under conditions where the dimer is only half-occupied (at low ATP concentrations), where the closed state is not very stable and the dimer spends more time in the apo state, and thus magnesium is the preferred divalent cation. It is currently not know what this half-occupied closed state looks like, and future work will have to visualize this state to answer how this half-occupied dimer can achieve a ˜10-fold higher ATP turnover rate.

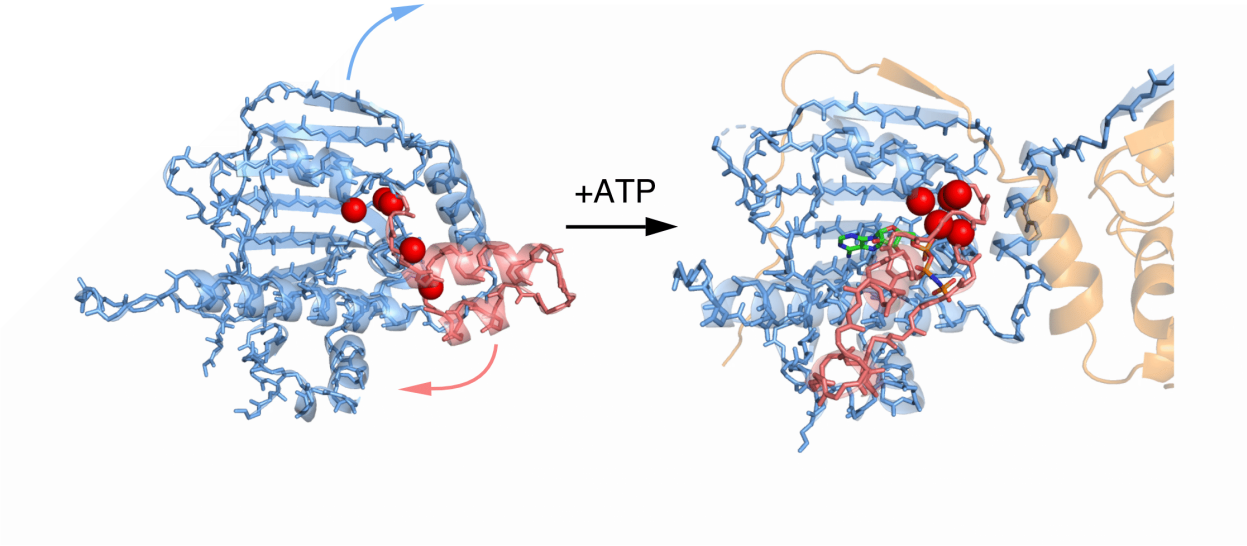

Figure 2.3: Molecular model for mechanism of calcium-binding in TRAP1. Molecular model of ATP-dependent calcium binding in TRAP1. The lid region (pink highlight) adopts an open state in absence of nucleotide (left cartoon diagram). The oxygen atoms involved in calcium binding (red spheres) do not form a cluster in the apo state. Once ATP binds the NTD, conformational changes within the base of lid re-arranges these oxygen atoms and the α-phosphate from the ATP provides the last oxygen to coordinate the calcium in an octahedral geometry. The movement of the lid (pink arrow) from open to closed is accompanied by the strand swap (black arrow) that stabilizes interactions between NTDs (transparent blue and orange cartoon). In this model, the calcium-binding sites are only formed once ATP fully occupy both sites and the NTDs are dimerized, explaining the apparent cooperativity in presence of calcium.

In principle, since calcium ions bind at an orthogonal site from magnesium, binding of both divalent cations may be possible. Preliminary experiments have shown that there are no significant effects when calcium is added to magnesium-ATPase reaction or vice-versa. By contrast, a few mitochondrial dehydrogenases have been found to be stimulated by calcium in the range between 0.1-10 μM[12], connecting their role in increasing ATP production. It remains to be seen how TRAP1's preferences for magnesium versus calcium under different ATP concentrations becomes physiologically relevant. One can imagine a scenario where ATP level gets low, down to tens of μM, in the mitochondrial matrix (e.g. high energy demand conditions where ATP need to be exported out to the cytoplasm) or high stress conditions where ATP is retained in the matrix. An

intriguing connection to calcium homeostasis in the mitochondria is perhaps how TRAP1 may be connected to the mitochondrial Permeability Transition Pore (mPTP)[9], which happens when the cell experiences Ca^{2+} overload and trigger apoptosis[23]. While the physiological context in which this calcium and magnesium regulation is not yet known, the findings in this work should provide a good starting molecular model to inform future work in elucidating the role of TRAP1 in the mitochondria.

2.5 Materials and methods

Protein purification

Full-length wild-type hTRAP1 and zTRAP1 (without mitochondrial signal sequence) was cloned into a pET151DTOPO vector as described previously[10]. Point mutation (D158N in hTRAP1) was introduced via site-directed mutagenesis by polymerase chain reaction. Protein was expressed in BL21(DE3)-RIL *E. coli* cells grown in TB media by addition of 0.5 mM IPTG at OD600 ˜0.8, then incubated with shaking for 12-18 hours overnight at 16°C. All of the TRAP1 constructs have an N-terminal 6xHis-tag with a cleavable TEV-site. Purification follows a standard protocol for an Ni-NTA chromatography using 40 mM Tris pH 8.0 buffer instead of phosphate, followed by an anion exchange with a MonoQ column, and a final size-exclusion step with an S200 superdex column.

ATPase assays

Most of the ATPase assays performed in this study uses the phosphate release assay as previously described [4] using a coumarin-labeled phosphate binding protein (PBP)[7]. Fluorescence was measured using a SpectraMax M5 plate reader by exciting at 385 nm and measuring emission at 475 nm with a cutoff filter at 455 nm at 'Low' sensitivity setting. The ATPase assays with zebrafish TRAP1 also monitors phosphate release via a chromogenic substrate 7-methylthioguanosine (7-MESG) in presence of an *E. coli* PNPase (purine nucleoside phosphorylase). In these assays, 0.14 mM 7-MESG and 2 μM PNPase was used per reaction. The net absorbance of 7-MESG was measured by subtracting absorbance at 500 nm from 354 nm. Both the PBP and PNPase used in this study was expressed and purified as previously described[4]. Initial rates from phosphate release assays were from obtained from fitted slopes of a linear function, $y = mx + b$, to the most linear region of each kinetic trace. The activity vs. concentration curves were analyzed by a standard Michaelis-Menten equation with the Hill-coefficient, n:

$$V_0 = V_{\max} \frac{[ATP]^n}{[ATP]^n + K_{0.5}^n} + \text{baseline}$$

For the two-site ATPase activity in wild-type TRAP1 in magnesium, the following equation was used:

$$V_0 = \frac{V_{\text{singleATP}} \frac{2[ATP]}{K_{\text{singleATP}}} + V_{\text{doubleATP}} \frac{[ATP]^2}{K_{\text{singleATP}} K_{\text{doubleATP}}}}{1 + \frac{2[ATP]}{K_{\text{singleATP}}} + \frac{[ATP]^2}{K_{\text{singleATP}} K_{\text{doubleATP}}}}$$

Where $K_{\text{singleATP}}$ and $K_{\text{doubleATP}}$ corresponds to apparent affinity constants at which half-maximum activity is achieved, and $V_{\text{singleATP}}$ and $V_{\text{doubleATP}}$ is the estimated maximum activity corresponding to 1 ATP-bound (half-occupied) and 2 ATP-bound (fully-occupied) TRAP1 dimer.

Crystallography and data processing

Zebrafish TRAP1 was incubated with 2 mM AMPPNP in presence of 5 mM MgCl2 at 5 mg/mL protein concentration. The reaction was incubated for at least 1 hour at 30°C to allow accumulation of the closed state prior to crystallization trials. Sitting drop reactions plate were set by mixing the protein with the crystallization solution (17% PEG-3350, 0.2 M Na/K tartrate, 36 mM hexammine cobalt) at 1:1 volume ratio (1 μL each) using a 15-well plate. Crystals grew in 2-3 days at room temperature. All diffraction data were collected at beamline 8.3.1 at the Advanced Light Source in Berkeley, CA. Two wavelengths were used for the anomalous data collections: 11111 eV (1.116 Å) and 7450 eV (1.66 Å). Datasets were indexed using XDS[8]. The native dataset collected at shorter wavelength solved using molecular replacement of TRAP1 in the closed state[10]. Structures were refined using REFMAC5[13] as part of the CCP4i package[21]. Anomalous difference map was generated using the program ANODE[19] using input files generated by the program SHELXC[16] and the solved structure without the calcium atoms.

2.6 Supplemental Figures

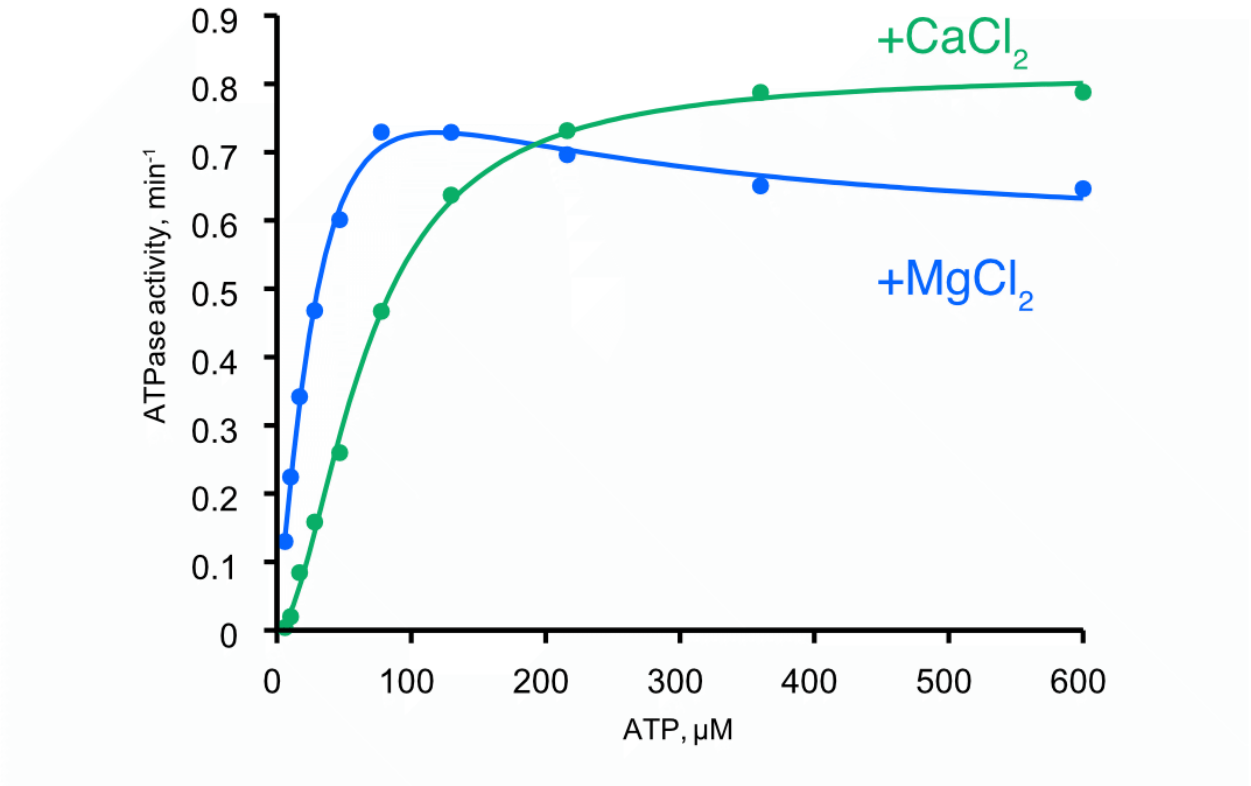

Figure S2.1: ATPase activity of zebrafish TRAP1 in presence of magnesium or calcium. Steady-state ATPase activity of zebrafish TRAP1 in presence of magnesium (blue) or calcium (green) measured at 30°C as a function of ATP concentration.

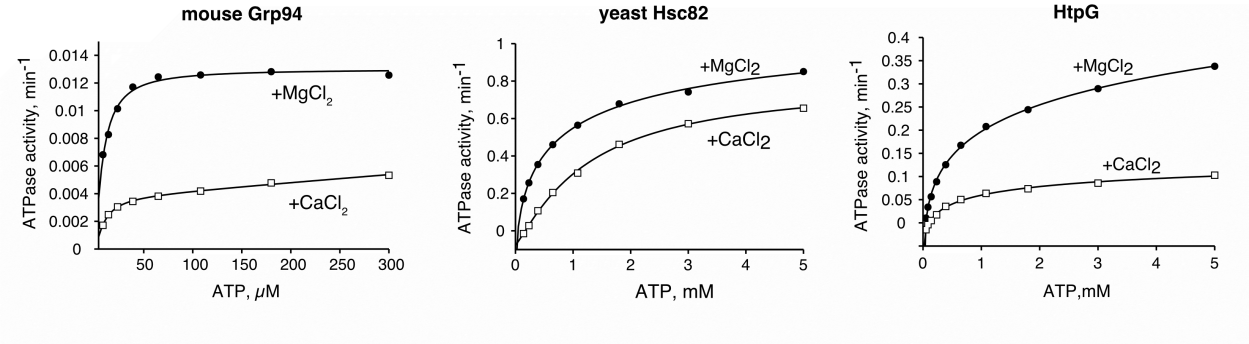

Figure S2.2: ATPase activities of Hsp90 homologs in presence of magnesium or calcium.Steady-state ATPase assays as a function of ATP concentration in presence of magnesium (filled circles) or calcium (empty black squares) of: full-length mouse endoplasmic reticulum (ER) Hsp90, Grp94 (left panel) measured at 25°C. Yeast Hsc82 (middle panel) at 30°C, and HtpG (right panel) at 30°C. For all of the experiments, the concentration of divalent cation is kept constant at 1 mM for Grp94 and 5 mM for yHsc82 and HtpG.

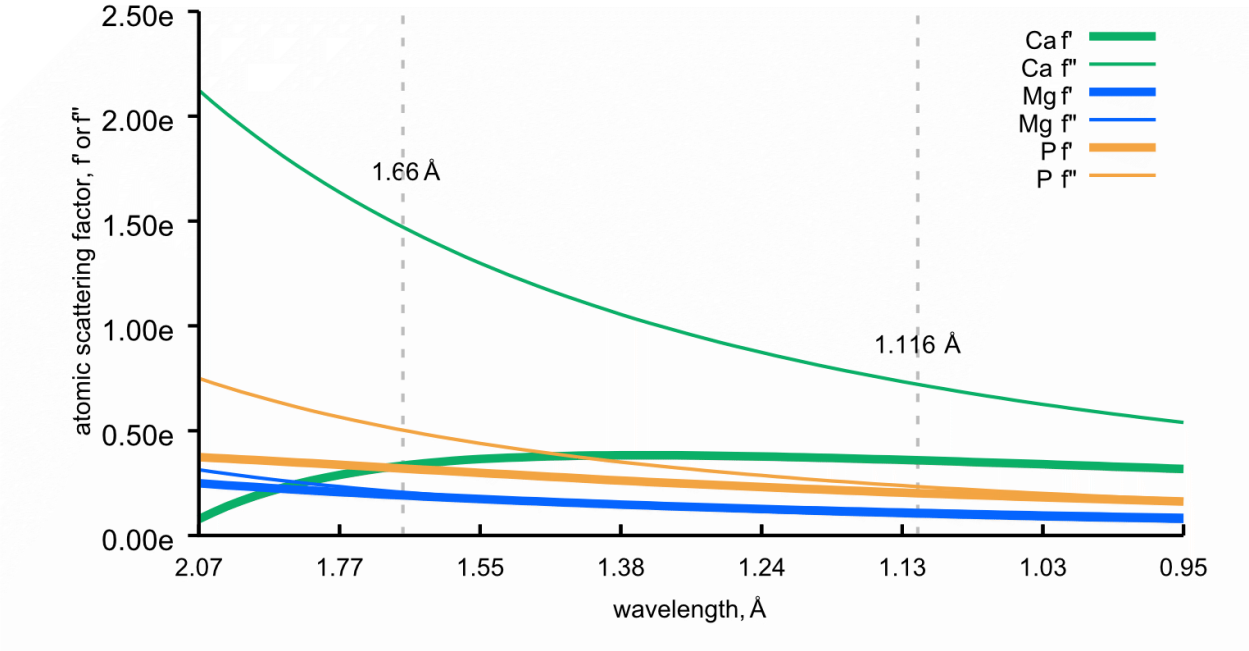

Figure S2.3: Anomalous X-ray scattering of calcium, magnesium, and phosphorus. The anomalous atomic scattering factor as a function of X-ray energy/wavelength in Å. The f' is shown in thin lines and f'' is shown as thick lines for calcium (green), magnesium (blue), and phosphorus (orange). In dashed gray line are two wavelengths used to collect anomalous datasets to generate anomalous density map from ANODE. One at the longer wavelength (1.66 Å) and one native dataset at 1.116 Å.

	hTRAP1, MgCl2	hTRAP1, CaCl2	zTRAP1, MgCl2	zTRAP1, CaCl2
V_{max}	-	0.67 ± 0.01	-	0.82 ± 0.01
$V_{\text{singleATP}}$	0.68 ± 0.05	-	1.50 ± 0.24	-
$V_{\text{doubleATP}}$	0.37 ± 0.02	-	0.56 ± 0.03	-
$K_{0.5}$	-	56.1 ± 2.2	-	66.2 ± 2.5
$K_{\text{singleATP}}$	58.0 ± 7.8	-	126.3 ± 30.5	-
$K_{\text{doubleATP}}$	38.0 ± 19.9	-	25.2 ± 12.7	-
n	-	1.4 ± 0.0	-	1.8 ± 0.1

Table 2.1: Fitted parameters for ATP titration kinetics with excess divalent cation

	zTRAP1, MgCl2	zTRAP1, CaCl2	zTRAP1, MgCl2	zTRAP1, CaCl2
	Low ATP (50 μM)		High ATP (400 μM)	
V_{max}	0.47 ± 0.09	0.29 ± 0.01	0.49 ± 0.02	0.62 ± 0.02
$K_{0.5}$	38.6 ± 15.0	66.1 ± 5.0	258.9 ± 15.1	37.1 ± 1.6
n	0.9 ± 0.1	1.2 ± 0.1	1.6 ± 0.1	1.9 ± 0.1

	hTRAP1, MgCl2	hTRAP1, CaCl2	hTRAP1, MgCl2	hTRAP1, CaCl2
	Low ATP (35 μM)		High ATP (350 μM)	
V_{max}	0.24 ± 0.00	0.16 ± 0.00	0.27 ± 0.02	0.37 ± 0.02
$K_{0.5}$	32.9 ± 1.8	91.9 ± 3.7	58.8 ± 10.5	13.4 ± 1.2
n	1.0 ± 0.0	1.1 ± 0.0	0.7 ± 0.1	1.7 ± 0.2

Table 2.2: Fitted parameters for divalent cation titration kinetics in low and high ATP

	MgCl2	CaCl2
V_{max}	3.77 ± 0.06	2.31 ± 0.15
$K_{0.5}$	72.5 ± 4.4	273.2 ± 29.2

Table 2.3: Fitted parameters for ATP titration kinetics in wildtype:D158N human TRAP1 heterodimer mixture

*ATPase activities have been normalized to protein (ATPase) concentration, reaction rates V are in $\mu M \text{ ATP} \cdot \text{min}^{-1}/\mu M \text{ protein}$ and concentration constants K are in μM.

References

1. Choe, H., Burtnick, L. D., Mejillano, M., Yin, H. L., Robinson, R. C. & Choe, S. The calcium activation of gelsolin: insights from the 3Å structure of the G4–G6/actin complex. *Journal of molecular biology* **324,** 691–702 (2002).

2. Cunningham, C. N., Krukenberg, K. A. & Agard, D. A. Intra- and Intermonomer Interactions Are Required to Synergistically Facilitate ATP Hydrolysis in Hsp90. *Journal of Biological Chemistry* **283,** 21170–21178 (July 2008).

3. Denton, R. M. Regulation of mitochondrial dehydrogenases by calcium ions. *Biochimica et Biophysica Acta (BBA)-Bioenergetics* **1787,** 1309–1316 (Nov. 2009).

4. Elnatan, D., Betegon, M., Liu, Y., Ramelot, T., Kennedy, M. A. & Agard, D. A. Symmetry broken and rebroken during the ATP hydrolysis cycle of the mitochondrial Hsp90 TRAP1. *eLife* **6,** e25235 (July 2017).

5. Frey, S., Leskovar, A., Reinstein, J. & Buchner, J. The ATPase cycle of the endoplasmic chaperone Grp94. *The Journal of biological chemistry* **282,** 35612–35620 (Dec. 2007).

6. Gout, E., Rébeillé, F., Douce, R. & Bligny, R. Interplay of Mg2+, ADP, and ATP in the cytosol and mitochondria: unravelling the role of Mg2+ in cell respiration. *Proceedings of the National Academy of Sciences* **111,** E4560–7 (Oct. 2014).

7. Hirshberg, M., Henrick, K., Haire, L. L., Vasisht, N., Brune, M., Corrie, J. E. & Webb, M. R. Crystal structure of phosphate binding protein labeled with a coumarin fluorophore, a probe for inorganic phosphate. *Biochemistry* **37,** 10381–10385 (July 1998).

8. Kabsch, W. & IUCr. XDS. *Acta crystallographica. Section D, Biological crystallography* **66,** 125–132 (Feb. 2010).

9. Kang, B. H., Plescia, J., Dohi, T., Rosa, J., Doxsey, S. J. & Altieri, D. C. Regulation of tumor cell mitochondrial homeostasis by an organelle-specific Hsp90 chaperone network. *Cell* **131,** 257–270 (Oct. 2007).

10. Lavery, L. A., Partridge, J. R., Ramelot, T. A., Elnatan, D., Kennedy, M. A. & Agard, D. A. Structural asymmetry in the closed state of mitochondrial Hsp90 (TRAP1) supports a two-step ATP hydrolysis mechanism. *Molecular Cell* **53,** 330–343 (Jan. 2014).

11. Leskovar, A., Wegele, H., Werbeck, N. D., Buchner, J. & Reinstein, J. The ATPase cycle of the mitochondrial Hsp90 analog Trap1. *The Journal of biological chemistry* **283,** 11677–11688 (Apr. 2008).

12. McCormack, J. G., Halestrap, A. P. & Denton, R. M. Role of calcium ions in regulation of mammalian intramitochondrial metabolism. *Physiological Reviews* (Apr. 1990).

13. Murshudov, G. N., Vagin, A. A., Dodson, E. J. & IUCr. Refinement of Macromolecular Structures by the Maximum-Likelihood Method. *Acta crystallographica. Section D, Biological crystallography* **53,** 240–255 (May 1997).

14. Partridge, J. R., Lavery, L. A., Elnatan, D., Naber, N., Cooke, R. & Agard, D. A. A novel N-terminal extension in mitochondrial TRAP1 serves as a thermal regulator of chaperone activity. *eLife* **3** (2014).

15. Richter, K., Soroka, J., Skalniak, L., Leskovar, A., Hessling, M., Reinstein, J. & Buchner, J. Conserved conformational changes in the ATPase cycle of human Hsp90. *The Journal of biological chemistry* **283,** 17757–17765 (June 2008).

16. Sheldrick, G. M. Experimental phasing with SHELXC/D/E: combining chain tracing with density modification. *Acta crystallographica. Section D, Biological crystallography* **66,** 479–485 (Apr. 2010).

17. Southworth, D. R. & Agard, D. A. Species-Dependent Ensembles of Conserved Conformational States Define the Hsp90 Chaperone ATPase Cycle. *Molecular Cell* **32,** 631–640 (Dec. 2008).

18. Sriram, M., Osipiuk, J., Freeman, B., Morimoto, R. & Joachimiak, A. Human Hsp70 molecular chaperone binds two calcium ions within the ATPase domain. *Structure (London, England : 1993)* **5,** 403–414 (Mar. 1997).

19. Thorn, A. & Sheldrick, G. M. ANODE: anomalous and heavy-atom density calculation. *Journal of Applied Crystallography* **44,** 1285–1287 (Nov. 2011).

20. Whitesell, L. & Lindquist, S. L. HSP90 and the chaperoning of cancer. *Nature Reviews Cancer* **5,** 761–772 (Oct. 2005).

21. Winn, M. D. *et al.* Overview of the CCP4 suite and current developments. *Acta crystallographica. Section D, Biological crystallography* **67,** 235–242 (Apr. 2011).

22. Wolf, S. G., Mutsafi, Y., Dadosh, T., Ilani, T., Lansky, Z., Horowitz, B., Rubin, S., Elbaum, M. & Fass, D. 3D visualization of mitochondrial solid-phase calcium stores in whole cells. *eLife* **6,** e29929 (Nov. 2017).

23. Zamzami, N. & Kroemer, G. The mitochondrion in apoptosis: how Pandora's box opens. *Nature reviews. Molecular cell biology* **2,** 67 (Jan. 2001).

Publishing Agreement

It is the policy of the University to encourage the distribution of all theses, dissertations, and manuscripts. Copies of all UCSF theses, dissertations, and manuscripts will be routed to the library via the Graduate Division. The library will make all theses, dissertations, and manuscripts accessible to the public and will preserve these to the best of their abilities, in perpetuity.

Please sign the following statement:

I hereby grant permission to the Graduate Division of the University of California, San Francisco to release copies of my thesis, dissertation, or manuscript to the Campus Library to provide access and preservation, in whole or in part, in perpetuity.

David Ebrahimian

Author Signature

12/22/2017

Date